Metal-Metal Interaction in Fischer Carbene Complexes – A Study on Ferrocenyl and Biferrocenyl Tungsten Alkylidene Complexes

Belinda van der Westhuizen,[a] J. Matthäus Speck,[b] Marcus Korb,[b] Joachim Friedrich,[c] Daniela I. Bezuidenhout[a*] and Heinrich Lang[b*]

[a]Chemistry Department, University of Pretoria, Private Bag X20, Hatfield 0028, South Africa.

[b]Technische Universität Chemnitz, Fakultät für Naturwissenschaften, Institut für Chemie, Anorganische Chemie, D-09107 Chemnitz, Germany.

[c]Technische Universität Chemnitz, Fakultät für Naturwissenschaften, Institut für Chemie, Theoretische Chemie, D-09107 Chemnitz, Germany.

ABSTRACT: A series of ferrocenyl (Fc = ferrocenyl; fc = ferrocen-1,1'-diyl) and biferrocenyl (Bfc = 1',1''-biferrocenyl; bfc = 1',1''-biferrocen-1,1'''-diyl) mono- and biscarbene tungsten(0) complexes of the type $[(CO)_5W=C(OMe)R]$ (**1**, R = Fc; **3**, R = Bfc) and $[(CO)_5W=C(OMe)\text{-}R'\text{-}(OMe)C=W(CO)_5]$ (**2**, R' = fc; **4**, R' = bfc) were synthesized according to the classical synthetic methodology by reacting $W(CO)_6$ with LiR (R = Fc, fc, bfc), followed by a subsequent alkylation using methyl trifluoromethanesulfonate. Electrochemical investigations were carried out on these complexes to get a closer insight into the electronic properties of **1** - **4**. The ferrocenyl and biferrocenyl moieties in **1** – **4** show reversible one electron redox events. It was further found that the Fischer carbene unit is reducible in an electrochemical one electron transfer process. For the tungsten carbonyl moieties, irreversible oxidation processes were found. In addition, charge transfer studies were performed on **1** - **4** by the use of *in situ* UV-Vis-NIR and infrared spectroelectrochemical techniques. During the UV-Vis-NIR investigations typical low energy transitions for the mixed-valent biferrocenyl unit were found. A further observed high energy NIR absorption is attributed to a metal-metal charge transfer transition between the tungsten carbonyl fragment and the ferrocenyl/biferrocenyl group in the corresponding oxidized states, which can be described as class II systems according to Robin and Day. This assignment was verified by infrared spectroelectrochemical studies. The electrochemical investigations are supported by DFT calculations. The structural properties of **1** - **4** in the solid state were investigated by single-crystal X-ray diffraction studies showing no substituent effects on bond lengths and angles. The biferrocenyl derivatives exhibit *syn*-conformation of the ferrocenyl and carbene building blocks.

KEYWORDS Spectroelectrochemistry, metal-metal interaction, ferrocene, biferrocene Fischer carbene complexes

INTRODUCTION

Since the first synthesis of transition metal alkyidene complexes of type $(CO)_5M=C(OMe)R$ (M = Cr, W) by Fischer and Maasböl in the early-1960s, this family of compounds received popularity, as they are fascinating molecules and powerful tools in organic and organometallic chemistry.[1] The Dötz benzannulation reaction and the Aumann reaction procedure, a simple approach to metallaolefins, are examples of their varied application in chemistry.[2] By incorporating a ferrocenyl substituent with known applications in molecular sensors,[3] energy transfer processes[4] and anti-cancer drugs,[5] the application of Fischer carbene complexes could be extended beyond their traditional use as ligands employed for organic transformations[6] and as auxiliary ligands in catalysis,[7] to design new push-pull systems with interesting non-linear optical (NLO) properties.[8] It is well known that the ferrocenyl moiety as a redox-active group displays high stability in the neutral as well as the oxidized state during one-electron transfer processes.[9] Such ferrocenyl systems are ideal for studying electronic interactions by applying electrochemical and spectroelectrochemical techniques; these are efficient instruments to investigate charge transfer transitions between the separated metal entities.[10] This phenomenon is almost unexplored in Fischer carbene complexes.[11] Moreover, studies in general concerning ferrocenyl- and biferrocenyl-functionalized Fischer carbene complexes are limited in the literature.[12,13]

We report herein the synthesis and characterization of a series of ferrocenyl (**1**, **2**) and biferrocenyl (**3**, **4**) tungsten(0) Fischer carbene complexes. Concerning the investigation of charge transfer transitions between the metallocenyl increments and the Fischer carbene units, the electrochemical and spectroelectrochemical properties of these species are discussed. These investigations are supported by computational studies.

Results and Discussion

Synthesis and Characterization. The tungsten Fischer carbene complexes **1** – **4** were prepared using the classical Fischer carbene synthetic methodology in which $W(CO)_6$ was reacted with LiR (R = Fc, fc, bfc; Fc = ferrocenyl, fc = ferrocen-1,1'-diyl, bfc = 1',1''-biferrocen-1,1'''diyl) to form the corresponding metal acylate, followed by a subsequent alkylation via addition of methyl trifluoromethanesulfonate (MeOTf) (Scheme 1, Experimental Section). Complex **1** has been previously prepared,[14] but single X-ray diffraction data have not been reported.

The lithiated ferrocenyl/biferrocenyl species were generated *in situ* from ferrocene or dibromobiferrocene by lithiation or lithium-bromine exchange reaction according to literature procedures (Scheme 1). [15,16] After purification by column chromatography, complexes **1** - **4** could be isolated as deep red to dark maroon solids and are very stable in the solid state as well as in solution toward moisture and air.

Complexes **1** - **4** were characterized by elemental analysis, IR and NMR (^1H, $^{13}C\{^1H\}$) spectroscopy, X-ray diffraction and mass spectrometry. Electronic effects of the carbene substituents can be followed in solution by IR and especially NMR spectroscopy. The electron withdrawing effect of the pentacarbonyl metal carbene moiety leads to a significant downfield shift of the resonances for the H_α protons (Figure 1) in **1** – **4** (4.80 – 5.00 ppm), compared to the value for ferrocene (4.15 ppm).[17] This is attributed to the π-delocalization of the positive formal charge onto the ferrocenyl substituent which aids in stabilizing the electrophilic carbene carbon atom, in addition to its inductive donating effect (Figure 1).

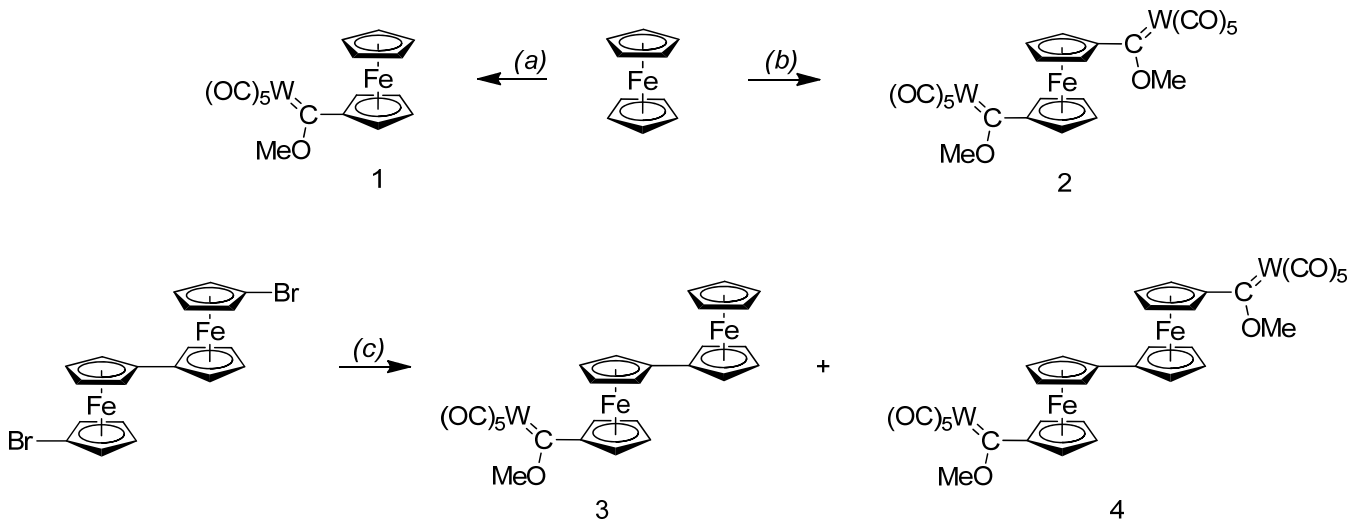

Scheme 1. Reaction conditions: (a) (i) tetrahydrofuran (thf), -80 °C, 1.06 eq ^{t}BuLi, 1 eq $W(CO)_6$; (ii) dichloromethane (CH_2Cl_2), -50 °C, 3 eq MeOTf. (b) (i) *n*-hexane, 2 eq ^{n}BuLi/TMEDA (1:1); (ii) thf, -60 °C, 2 eq $W(CO)_6$; (iii) CH_2Cl_2, -30 °C, 6 eq MeOTf. (c) (i) thf, -40 °C, 2.0 eq ^{n}BuLi; (ii) 2 eq $W(CO)_6$; (iii) CH_2Cl_2, -30 °C, 6 eq MeOTf.

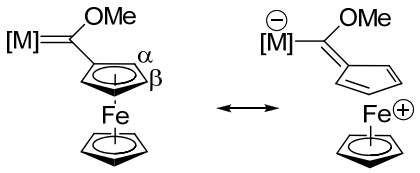

Figure 1. Stabilization of Fischer carbene complexes with a ferrocenyl group.

A comparison of the H_α ^{1}H NMR signals between complexes **1** – **4** as well as the ν(CO) stretching frequencies (A_1") reveal no significant differences, due to similarity of the carbene complexes (Table 1).

Electrochemistry and Molecular Orbital Analysis. The electrochemical studies of Fischer carbene complexes **1** – **4** were carried out under an argon atmosphere in dichloromethane solutions containing $[N^{n}Bu_4][B(C_6F_5)_4]$ (0.1 M) as supporting electrolyte and were supported by DFT calculations (computational details are given in the Experimental Section). Spectroelectrochemical investigations of **1** - **4** were carried out using an OTTLE[18] (= Optically Transparent Thin Layer Electrochemistry) cell (Experimental Section).

During the electrochemical studies of **1**, three significant redox events could be observed. One reversible event was detected for **1** at $E^{0'}$ = 300 mV, similar as detected previously,[11] which can be assigned to the ferrocenyl/ferrocenium (Fc/Fc^+) redox process (Table 2, Figures 2 and SI-1). The significant anodic shift of this redox event, relative to ferrocene, demonstrates the electron withdrawing effect of the Fischer carbene moiety. Computational studies were carried out to verify the nature of the observed redox processes. The solvent effects on the ionization energies were taken into account with the conductor like screening model (COSMO) using ε = ∞ (Table 3, Figure 3).

Table 1. Selected NMR data and the infrared ν(CO) stretching frequencies (A_1") of Fischer carbenes **1** – **4** (Figure SI-5).

Compd.	H_α δ ^{1}H [ppm]	$C_{carbene}$ δ $^{13}C\{^1H\}$ [ppm]	A_1"ν(CO) [cm^{-1}]
1	4.99	307.73	2063
2	5.01	310.72	2063
3	4.83	307.36	2062
4	4.83	308.72	2062

As a result from the DFT calculations, the oxidation potential for the first oxidation in **1** was calculated to 0.3 V (Table 3). Considering the moderate level of theory, the theoretical value is in good agreement compared with the experimental value ($E_{ox\text{-}onset}$ = 0.22 V) as well as with other considerations regarding a correlation between the electrochemical measurement and ionization energies.[19]

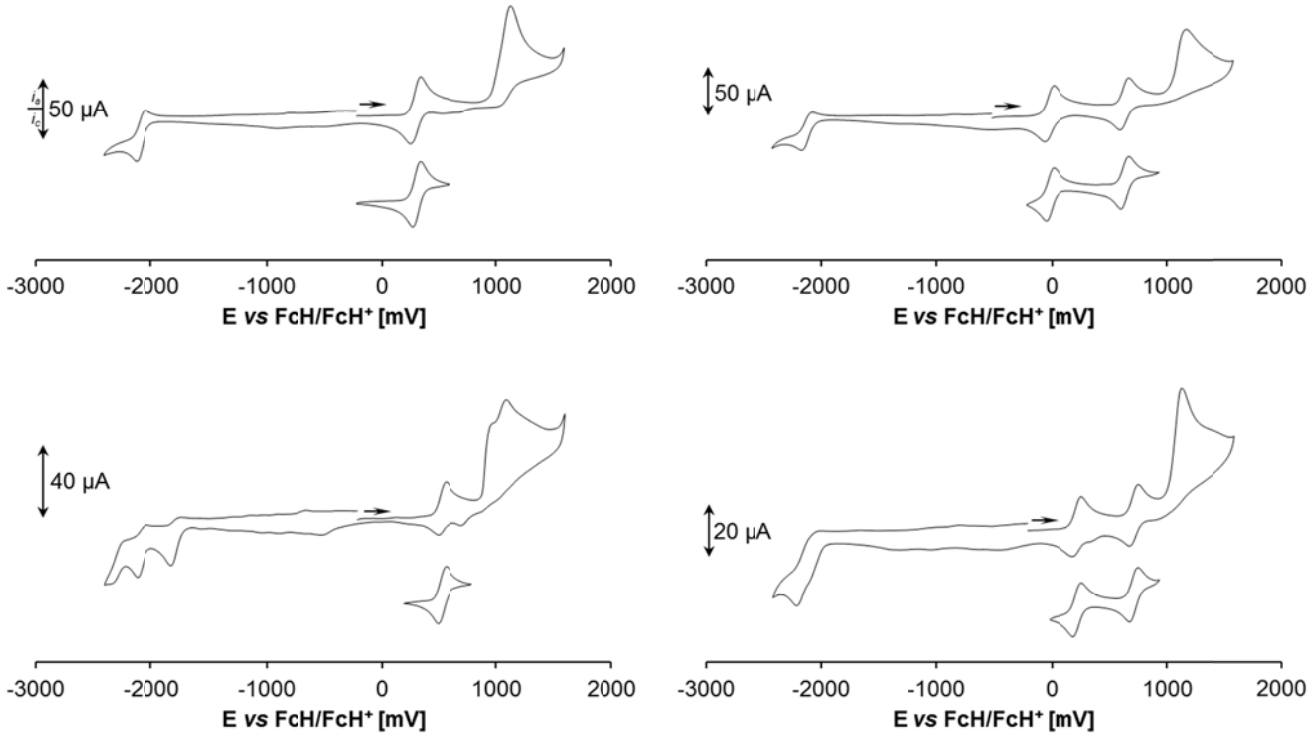

Figure 2. Cyclic voltammograms of Fischer carbenes **1** (left top), **2** (left bottom), **3** (right top) and **4** (right bottom). Scan rate: 100 mVs^{-1} in dichloromethane solutions (1.0 $mmol{\cdot}L^{-1}$) at 25 °C, supporting electrolyte $[N^nBu_4][B(C_6F_5)_4]$ (0.1 M). In case of the full range cyclic voltammograms the initial cycle is shown, arrows indicate the potential direction. For cyclic voltammetry data see Table 2.

Table 2. Cyclic voltammetry data (potentials *vs* FcH/FcH^+) of 1.0 $mmol{\cdot}L^{-1}$ solutions of **1** – **4** in dry dichloromethane containing $[N^nBu_4][B(C_6F_5)_4]$ (0.1 M) as supporting electrolyte at 25 °C. [a] i_{pa}/i_{pc}. [b] ΔE_{pc}.

Compd.	$E_{pa}/E_{pc}/\Delta E_p/E^{0'}/\Delta E^{0'}$ [mV] (i_{pc}/i_{pa}) Wave (no.)				
	(1)	(2)	(3)	(4)	(5)
1	-2053/-2133/80/ -2093 (0.46)[a]	266/334/68/ 300 (0.95)	1125/ -		
2	- /-2124	- /-1823/ 301[b]	554/484/70/ 519 (0.99)	989/ -	1086/ -
3	-2072/-2166/94/ -2119 (0.54)[a]	20/-48/68/-14 (0.98)	671/604/67/ 637/651 (0.98)	1161/ -	
4	- /-2213	- /-2100/ 113[b]	261/191/70/ 226 (0.99)	750/679/71/ 715/489 (0.98)	1127/ -

Table 3. Calculated ionization energies and oxidation/reduction potentials of **1** (computational details are given in the Experimental Section).
[a] The ionization energy of ferrocene was calculated to 4.3 eV (414.9 kJ/mol).

Compd.	B3LYP Ionization Energy [kJ/mol]	Incremental Ionization Energy [kJ/mol]	*E vs* FcH/FcH^+ [V][a]
$\mathbf{1}^-$	-273.7		
1	0.0	273.7	-1.5
$\mathbf{1}^+$	447.0	447.0	0.3
$\mathbf{1}^{2+}$	988.6	541.6	1.3
$\mathbf{1}^{3+}$	1632.8	644.2	2.4

Furthermore, the spin density distribution of $\mathbf{1}^+$ offers a localization (Mulliken spin density of 1.25) around the iron center and thus verifies the assignment to a Fc/Fc^+ redox event (*vide supra*, Figure 3).
Further increasing the potential leads to an irreversible oxidation process at E_{pa} = 1.13 V, which is associated with an oxidation of the tungsten carbonyl moiety (Figures 2 and SI-1). The peak current for this oxidation was observed as 2.5 times higher as for the ferrocenyl unit, similar as observed previously.[20] If an one step electrochemical process is assumed, the observed current reveals a two electron oxidation process, according to the Randles-Sevcik equation. However, the large differences between the calculated oxidation potentials (Table 3) suggest well-separated oxidation events during the generation of the oligocationic species. To determine the flown charge equivalents, chronocoulometric measurements were carried out. Assuming a reversible one electron redox event for the Fc/Fc^+ couple (1 eq), the charge equivalents can be determined from the slope of the Anson plot, charge (*Q*) *vs* square root of time ($t^{1/2}$), with the Anson equation.[21] For the tungsten oxidation a value of 2.9 eq was obtained and suggests an electrode mediated successive three electron oxidation process, formal from W(0) to W(III). Nevertheless, such results should be handled with caution, due to irreversibility of the oxidation process.
Furthermore, a partially reversible reduction (Figures 2 and SI-1) could be found in the cathodic end of the electrochemical window at E_{pc} = –2.09 V (theoretical value: *E* = -1.5 V, Table 3). This redox process is associated with a carbene center reduction/reoxidation process (Table 2, Figure 2).[22]

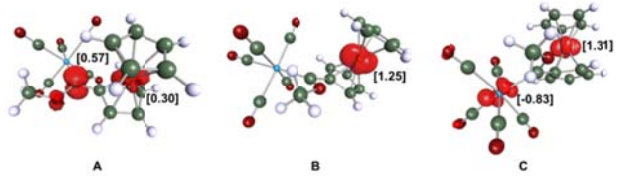

Figure 3. Computed spin density plots of $\mathbf{1}^-$ (**A**), $\mathbf{1}^+$ (**B**) and $\mathbf{1}^{2+}$ (**C**). For computational details see Experimental Section. Numbers in brackets indicate the computed Mulliken spin densities.

The cyclic voltammetric as well as the chronocoulometric (1.1 eq) studies suggest a one electron redox process. From the spin density distribution in Figure 3 (A) localization around the carbene carbon can be seen.
A further tungsten carbene substituent on the ferrocenyl unit (complex **2**) leads to an anodic shifting of the Fc/Fc^+ redox process to $E^{0'}$ = 519 mV. Within this context, the first carbene reduction should be easier than in **1** and was observed 170 mV less cathodic compared to the carbene reduction in the ferrocenyl monocarbene complex (Table 2, Figure 2). A second carbene reduction could be found at E_{pc} = –2.12 V, 300 mV more cathodic as the generation of $\mathbf{1}^-$ (Table 2, Figures 2 and SI-2). The observation of two separated carbene reduction events leads to the conclusion that the first reduction process has an influence on the second one, depending on the bridging unit (in comparison with **4**, *vide infra*). A similar observation was made during the oxidation events of the tungsten centers, where two separate peaks at E_{pa} = 0.99 V and 1.09 V were found (Table 2). The oxidation potentials of both the 1st processes were found to be more cathodic as observed for **1**.
In the case of the biferrocenyl Fischer carbene complex **3**, one redox event was detected at E_{pc} = –2.12 V and is also assigned to the carbene reduction electrode reaction (vide supra). For the biferrocenyl unit itself, two well separated ($\Delta E^{0'}$ = 651 mV) reversible one electron redox events at $E^{0'}$ = -14 mV and 637 mV were found (Table 2, Figure 2). A comparison of the first Bfc redox process with the corresponding event in biferrocene itself reveals an anodic shift of approx. 110 mV for the $\mathbf{3}/\mathbf{3}^+$ redox couple, only one third of that observed for the corresponding process in **1**.[22] Thus, the influence of the tungsten carbene moiety on the first biferrocenyl redox process in **3** is significantly lower than that on the ferrocenyl redox event in **1**. In addition, an oxidation peak at E_{pa} = 1.16 V was noticed and is assigned to the irreversible tungsten carbonyl oxidation (vide supra, Table 2, Figure 2). The electrochemical investigation of the biferrocenyl carbene complex **4** revealed two carbene reduction processes with a smaller separation (ΔE_{pc} = 113 mV) as observed for **2**, due to the larger biferrocenyl bridge between the Fischer carbene units (vide supra). For the biferrocenyl increment, two reversible redox events were observed, which are separated by $\Delta E^{0'}$ = 489 mV. Hence $\Delta E^{0'}$ is smaller as detected for biferrocene ($\Delta E^{0'}$ = 530 mV) under similar experimental conditions.[23] A comparison of formal potentials for the first biferrocenyl redox processes of compounds **3** and **4** shows again the anodic potential shift, due to the installation of a second Fischer carbene substituent. Finally, the irreversible oxidation of the tungsten carbonyl fragments was found at ΔE_{pa} = 1.13 V, even slightly more cathodic than for **3**. In order to get more insight into the oxidation processes of **1** - **4** spectroelectrochemical studies were carried out by a stepwise increase of the potential *vs* Ag/AgCl in an OTTLE cell (Optically Transparent Thin Layer Electrochemistry)[18] using a 0.1 M dichloromethane solution of $[N^nBu_4][B(C_6F_5)_4]$ as supporting electrolyte. This procedure allows the *in situ* generation of mixed-valent species such as $\mathbf{1}^+$, $\mathbf{2}^+$, $\mathbf{3}^{n+}$ and $\mathbf{4}^{n+}$ (n = 1, 2). If deconvolution of NIR absorptions was used, transitions with Gaussian shapes were taken to get fits good enough to allow an almost exact overlay of the

Table 4. NIR and infrared data of **1** – **4** in dry dichloromethane containing $[N^nBu_4][B(C_6F_5)_4]$ (0.1 M) as supporting electrolyte at 25 °C. [a] $\lambda = \nu_{max} - \Delta G^0$. [b] $\lambda = \nu_{max}$. [c] $\Delta G^0 = 5900\ cm^{-1}$. [d] $\Delta G^0 = 2420\ cm^{-1}$. [e] *Shoulder.* [f] *Neutral compound.*

Compd.	Transition	ν_{max} [cm^{-1}] (ε_{max} [$Lmol^{-1}cm^{-1}$])	$\Delta\nu_{1/2}$ [cm^{-1}]	$\Delta\nu_{1/2(theo)}$ [cm^{-1}] $\{\Delta\nu_{1/2(theo)} = (2310\lambda)^{1/2}\}$ [a]	ν_{CO} [cm^{-1}]
$\mathbf{1}^+$	MMCT	9270 (340)	4660	2790[c] (4630[b])	1956, 2076 (1931, 2063)[f]
	LF	3930 (50)	1280		
$\mathbf{2}^+$	MMCT	8000 (470)	5070	2200[c] (4300[b])	1959, 2071, 2080[e] (1937, 2063)[f]
	LF	3670 (70)	1010		
$\mathbf{3}^+$	MMCT	8930 (65)	2510	2650[c]	1935, 2065 (1930, 2061)[f]
	IVCT	5580 (930)	3640	2700[d] (3590[b])	
	IBT	3790 (340)	820	1780[d]	
$\mathbf{3}^{2+}$	MMCT	8190 (280)	4860	2300[c] (4140[b])	1958, 2077
	LF	3510 (120)	1590		
$\mathbf{4}^+$	MMCT	8870 (500)	3170	2620[c]	1941, 2065, 2071[e] (1930, 2063)[f]
	IVCT	4320 (1290)	3720	3160[b]	
	IBT	3320 (720)	900	2770[b]	
$\mathbf{4}^{2+}$	MMCT	7870 (570)	9030	2133[b] (4260[b])	1945, 2071
	LF	3600 (200)	700		

sum of the spectral components with the experimental spectra. All neutral Fischer carbene complexes do not display, as expected, any absorptions in the NIR range. The corresponding UV-Vis spectra are presented in the Supporting Information (Figures SI-3, SI-6 to SI-8). For calculation of the theoretical bandwidth at half height ($\Delta\nu_{1/2(theo)}$) in asymmetric systems, the energy gap between the diabatic states (ΔG^0) could be estimated, using the difference in oxidation potentials of the two redox sites. Regarding this, the oxidation potential of $(CO)_5W{=}C(OMe)Me$[20] as well as the formal potential of the $\mathbf{1}/\mathbf{1}^+$ redox process were used (Table 4). Furthermore, an experimental $\Delta\nu_{1/2}$ value equal or larger than the theoretical width for symmetrical systems verifies clearly a class II assignment according to Robin and Day, since theoretical $\Delta\nu_{1/2}$ values for asymmetrical systems are generally smaller as the corresponding widths for the symmetrical case.[24]

During the oxidation of **1** typical absorptions in the UV-Vis region of inner ferrocenyl transitions (π-π^* and MLCT/d-d) were observed (Supporting Information).[25] Upon successively increasing the potential, two main absorptions at 9270 cm^{-1} and 3930 cm^{-1} could be detected in the NIR range during the generation of $\mathbf{1}^+$ (in comparison with FcH^+, Table 4 and Figure 4).[26] The latter very weak absorption is attributed to an iron-based forbidden ligand field (LF) transition as described previously.[9f,10b,27] The weak high energy NIR absorption band at around 9300 cm^{-1} can be assigned to a metal-metal charge transfer transition (MMCT) between the tungsten carbonyl fragment and the ferrocenium unit. To verify an interaction between the tungsten and the ferrocenyl building blocks, infrared spectroelectrochemical measurements monitoring the shift of ν(CO) stretching frequencies during the oxidation process were carried out (Figures 5 and SI-4).

For carbene **1**, absorptions could be found at 1930 cm^{-1} and 2063 cm^{-1}, respectively (Experimental Section). Upon

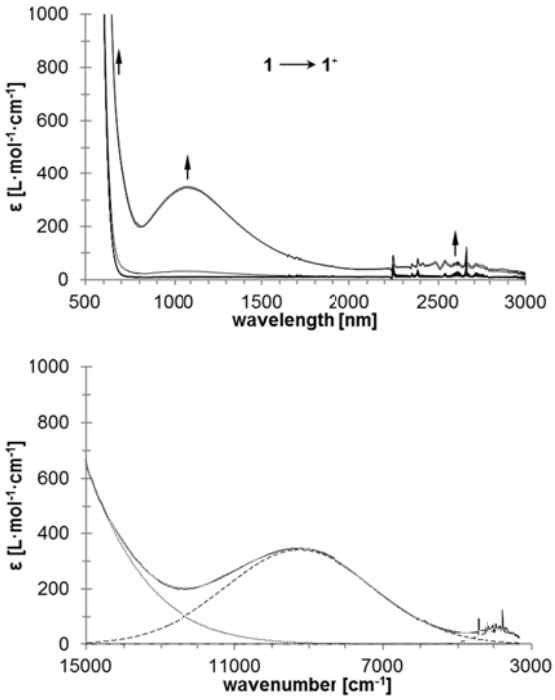

Figure 4. UV-Vis/NIR spectra of **1** at rising potentials (0 to 700 mV). Top: 500 – 3000 nm. Bottom: deconvolution of NIR absorptions at 700 mV using three distinct overlapping transitions with Gaussian shapes (dashed line indicates MMCT absorptions, dotted line corresponds to absorptions caused by interactions between ligand and metal, dotted-dashed line represents ligand field transitions). All potentials *vs* Ag/AgCl at 25 °C in dichloromethane, supporting electrolyte $[N^nBu_4][B(C_6F_5)_4]$ (0.1 M). Arrows indicate increasing or decreasing as well as shifting absorptions.

generation of the monocationic species $\mathbf{1}^+$ a decrease of these bands takes place together with an increase of absorptions at 1956 cm^{-1} and 2076 cm^{-1}, respectively (Table 4 and Figure 5, top left). The limited shift of the $W(CO)_5$ carbonyl stretching frequencies on oxidation is the result of conjugative and inductive effects that operate in stabilizing the positive charge on the iron nucleus
by the metal carbene. Hence, the reduced back-bonding abilities of the Fc^+ substituent to the carbonyl carbon atoms (compared to neutral Fc) leads to an increasing of the CO bond strengths and results in larger stretching frequencies (Figure 5). The observed carbonyl stretching frequencies are in good agreement with the calculated infrared spectra for **1** and the corresponding monocation (Figure SI-4). Moreover, the difference ($\Delta\nu$ = 13 cm^{-1}) between the two observed frequencies, 2063 cm^{-1} (**1**) and 2076 cm^{-1} ($\mathbf{1}^+$), for the total symmetrical carbonyl stretching mode (A_1", *vide supra*, Figure SI-5) differs only slightly from the corresponding value for the predicted vibrations of **1** and $\mathbf{1}^+$ ($\Delta\nu$ = 19 cm^{-1}, Figure SI-4, Table 4). Furthermore, the small magnitude of the carbonyl band shifts, compared to shifts of more than 100 cm^{-1} for a metal carbonyl-based oxidation, indicates an iron based oxidation process and a valence trapped situation in $\mathbf{1}^+$. Calculation of the spin density distribution for $\mathbf{1}^+$ confirms this conclusion (Figure 3). Thus, the interaction between the ferrocenyl unit and the tungsten carbene increment can be described with a weakly coupled class II system according to Robin and Day.[24]
The absorption behavior of $\mathbf{2}^+$ during the oxidation of molecule **2** is similar to the corresponding Fischer monocarbene complex **1** (Table 4, Figure SI-6). Absorptions at 3670 cm^{-1} and 8000 cm^{-1} could be noticed and are assigned to a ligand field transition and an electronic interaction between the tungsten carbene units and the iron center, too (MMCT, vide supra). The latter transition was observed as being more intense as the corresponding absorption for $\mathbf{1}^+$, due to the second Fischer carbene substituent on the ferrocenyl moiety. During the infrared spectroelectrochemical investigations of **2**, a band at 1959 cm^{-1} as well as a broad absorption at 2071 cm^{-1}, the carbonyl stretching frequency (A_1", *vide supra*), could be found upon generation of $\mathbf{2}^+$ (Figure 4, Table 4). However, the width of the latter band suggests a superposition of two absorptions close together (Figure 5) and would be consistent with a class II electronic coupling behavior according to Robin and Day (*vide supra*).[24] A comparison between the observed ($\Delta\nu_{1/2}$) and the calculated band width at half height ($\Delta\nu_{1/2(theo)}$) of the MMCT absorption supports this classification (Table 4).

An enhancement of ferrocenyl complex **1** to a biferrocenyl Fischer carbene complex **3** leads to an occurrence of two (Figure SI-7) absorptions in the NIR range during the generation of cation $\mathbf{3}^+$. Characteristic for biferrocenyl systems is the observation of an inter valence charge transfer (IVCT) band close together with another absorption on the low energy side of the ICVT absorption (Table 4, Figure SI-7). Tuczek *et al.* attributed this intrabiferrocenyl transition (IBT), around 3800 cm^{-1} for $\mathbf{3}^+$, to a further intervalence charge transfer transition.[26,29] However, the latter absorption is very narrow compared to the corresponding value of $\Delta\nu_{1/2(theo)}$ (Table 4, Figure SI-7). An assignment to a LMCT or a charge transfer assisted ligand field transition is also not uncommon.[25,30]
Furthermore, a similar absorption band, which was found for $\mathbf{1}^+$ and $\mathbf{2}^+$, attributed to an electronic interaction between the tungsten carbonyl moiety and the iron center, is observed as an ill-pronounced shoulder that could be resolved into a separate peak in a deconvolution procedure (Figure SI-7, Table 4). The infrared spectroelectrochemical investigations of **3** support this observation, since upon formation of $\mathbf{3}^+$ the initial ν(CO) frequencies (Table 4) shift by only a few wavenumbers to higher energies (1935 cm^{-1} and 2065 cm^{-1}, Figure 5). Thus, in combination with the electrochemical results, the first oxidation in **3** takes primarily place at the terminal ferrocenyl unit. During the generation of $\mathbf{3}^{2+}$ the low energy absorptions in the NIR range disappear and further transitions could be detected at 3510 cm^{-1} (LF) and around 8200 cm^{-1} (Table 4, Figure SI-7). The latter transition is also associated to a metal-metal charge transfer between the tungsten increment and the Bfc unit. The corresponding infrared absorption behavior during the formation of $\mathbf{3}^{2+}$ verifies this conclusion, similar as observed for $\mathbf{1}^+$ (*vide supra*, Figure 5).

A second tungsten Fischer complex fragment on the biferrocenyl building block leads to three NIR absorptions for monocationic $\mathbf{4}^+$ (Table 4, Figure 6). The two transitions at lower energies are typical for such mixed-valent biferrocenyl species (*vide supra*). The intensities are higher as observed for $\mathbf{3}^+$ but weaker than for symmetrical electron donor substituted biferrocenyl systems.[31] The third absorption around 8900 cm^{-1} can be assigned again to a MMCT transition, caused by an electronic interaction of the tungsten units with the biferrocenyl group in $\mathbf{4}^+$. Within the infrared spectroelectrochemical studies of **4**, a shifting of the initial ν(CO) stretching frequencies from 1930 cm^{-1} and 2063 cm^{-1} to formal 1941 cm^{-1} and 2065 cm^{-1} is characteristic, whereas an increase of a shoulder at 2071 cm^{-1} could be observed (Figure 5). This suggests a main localization of positive charge in the biferrocenyl fragment within the infrared timescale corresponding to a weakly coupled class II system according to Robin and Day.[24] Further oxidation to the dicationic $\mathbf{4}^{2+}$ leads to absorptions at 1945 cm^{-1} and an increasing band at 2071cm^{-1} (A_1"), thus the small magnitude of carbonyl band shift indicates again a limited delocalization of the positive charge between tungsten moieties and the iron centers (*vide supra*). This is consistent with the detection of an increasing NIR absorption at 7870 cm^{-1} (MMCT) upon decreasing of the low energy transitions, caused from intra biferrocenyl electronic interactions, during the formation of $\mathbf{4}^{2+}$ (Table 3, Figure 6). Finally, a very weak ligand field transition could be observed at 3600 cm^{-1}, similar as described previously (*vide supra*, Table 4 and Figure 6).[9f,10b,27]

Crystallography. The molecular structures of **1**[11,25] and **2** – **4** in the solid state have been determined by single-crystal X-ray diffraction analysis.

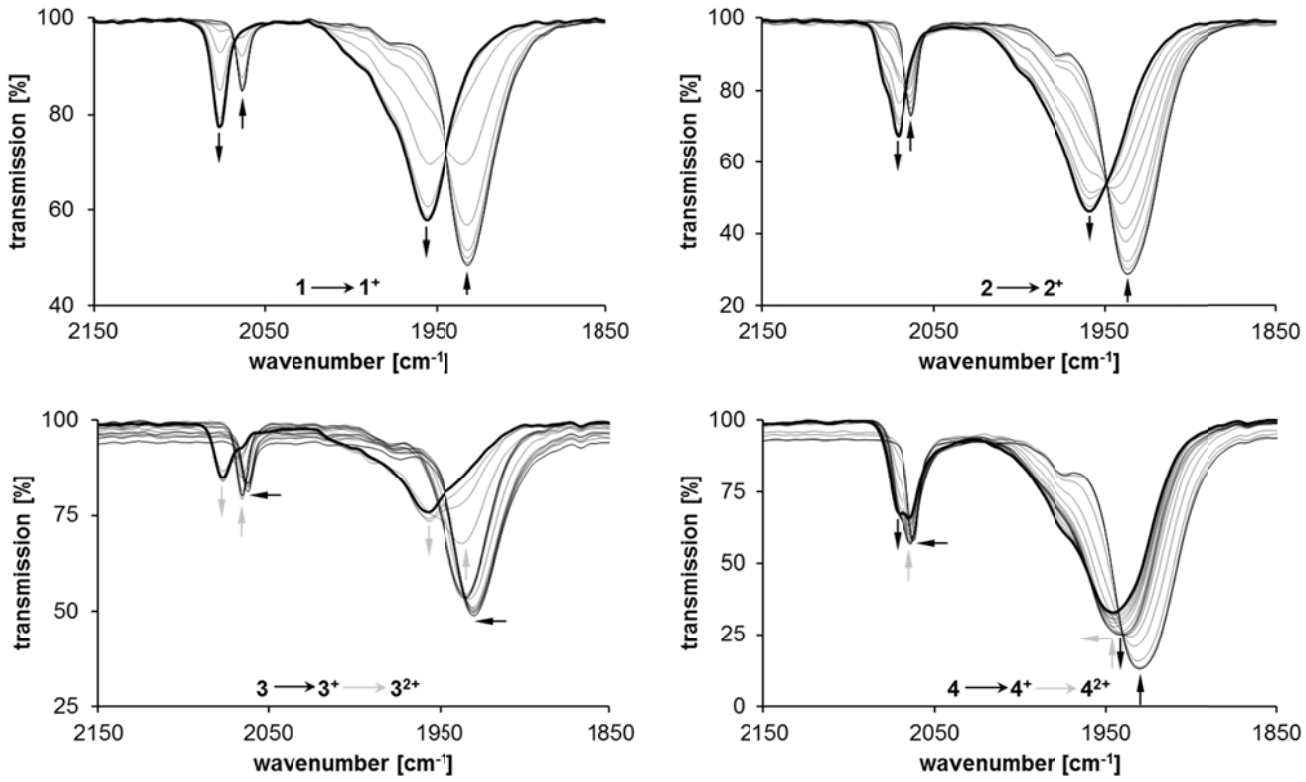

Figure 5. Infrared spectra of **1** - **4** at rising potentials (left top: -200 to 950 mV; right top: -200 to 1350 mV; left bottom: -100 to 1350 mV; right bottom: -100 to 1600 mV). All potentials *vs* Ag/AgCl at 25 °C in dichloromethane on 5 mM analyte solutions, supporting electrolyte $[N^nBu_4][B(C_6F_5)_4]$ (0.1 M). Arrows indicate increasing or decreasing as well as shifting absorptions.

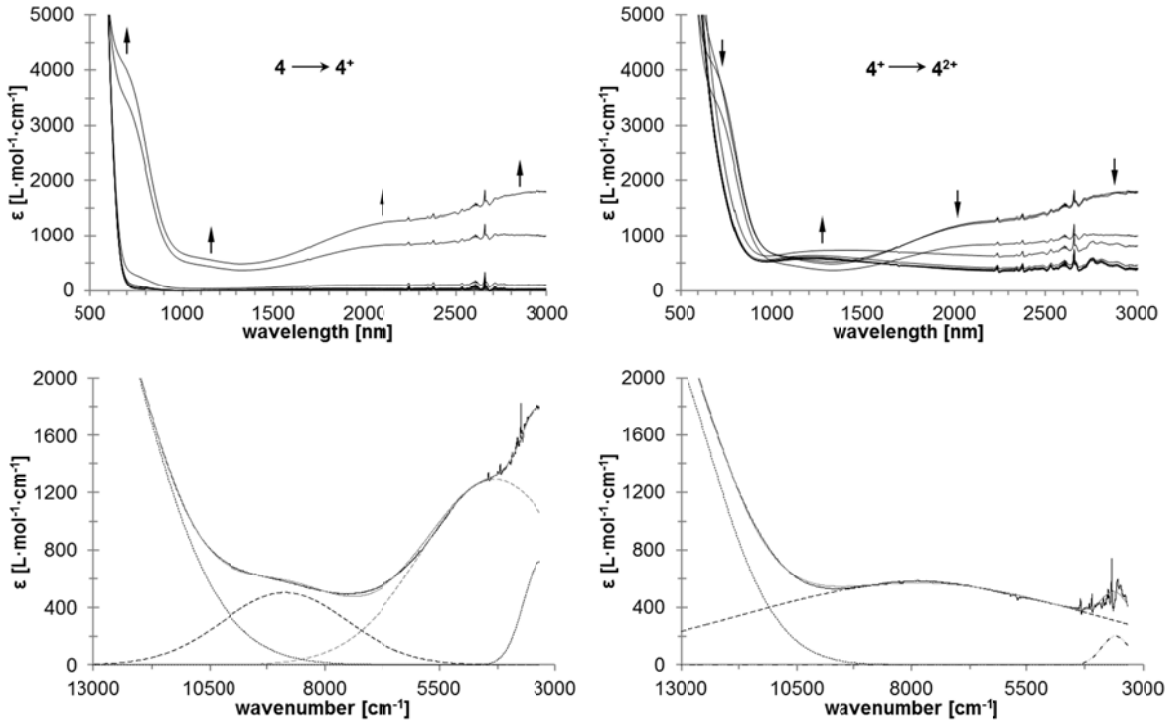

Figure 6. UV-Vis/NIR spectra of **4** at rising potentials (left: -100 to 600 mV; right: 600 to 1050 mV). Bottom (left): deconvolution of NIR absorptions at 600 mV using four distinct overlapping transitions with Gaussian shapes. Bottom (right): deconvolution of NIR absorptions at 1050 mV, using three distinct overlapping transitions with Gaussian shapes (dashed line indicates IVCT (grey) or MMCT (black) absorptions, dotted line corresponds to absorptions caused by interactions between ligand and metal (black) as

well as intrabiferrocenyl transitions (IBT, grey), dotted-dashed line represents ligand field transitions). All potentials *vs* Ag/AgCl at 25 °C in dichloromethane, supporting electrolyte $[N^nBu_4][B(C_6F_5)_4]$ (0.1 M). Arrows indicate increasing or decreasing as well as shifting absorptions.

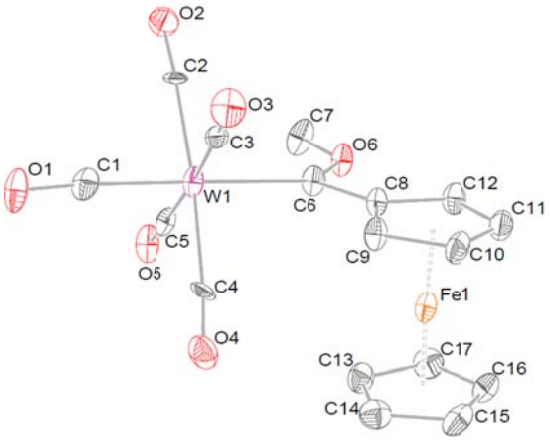

Figure 7. Single crystal X-ray structure analysis of **1** with the atom numbering scheme. Ellipsoids represent 50 % probability levels. Hydrogen atoms are omitted for clarity. Selected bond lengths (Å), angles (°), and torsion angles (°): W1–C1 1.981(14), W1-C6 2.211(13), C6-O6 1.339(15), C6-C8 1.458(19), D1–Fe1 1.652(19), D2–Fe1 1.656(17), O6-C6-W1 128.33(92), C8-C6-W1 126.39(93), O6-C6-C8 105.24(11), D1–Fe1–D2 176.77(18), C8–D1–D2–C13 –13.31(10), W1–C6–O6–C7 –1.67(19), C8–C6–O6–C7 –179.67(12), O6–C6–W1–C2 –46.63(13), C8–C6–W1–C2 –130.97(12), O6–C6–C8–C9 –178.96(14), W1–C6–C8–C9 3.00(21). D1: C8–C9–C10–C11–C12, D2: C13–C14–C15–C16–C17.

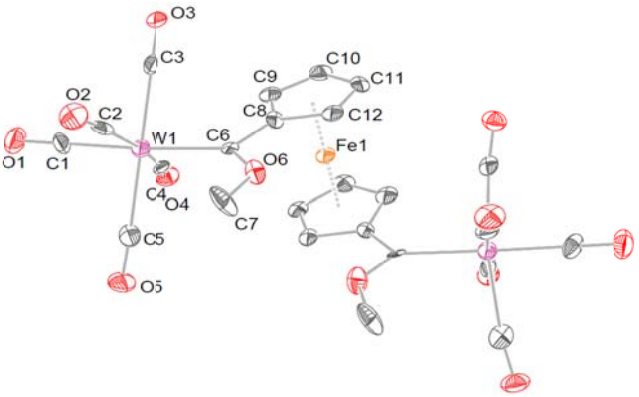

Figure 8. Single crystal X-ray structure analysis of **2** with the atom numbering scheme. Equivalent atoms are generated by the following symmetry operation: –x+1, y, –z+3/2. Ellipsoids represent 50 % probability levels. Disordered and hydrogen atoms are omitted for clarity. Selected bond lengths (Å), angles (°), and torsion angles (°): W1–C1 1.987(11), W1-C6 2.204(99), C6-O6 1.353(12), C6-C8 1.443(12), D1–Fe1 1.657, O6-C6-W1 127.84(57), C8-C6-W1 125.54(61), O6-C6-C8 106.49(81), D1–Fe1–D1_$1 176.95(12), C8–D1–D1_$1–C12_$1 3.69(63), W1–C6–O6–C7 –4.45(12), C8–C6–O6–C7 171.66(95), O6–C6–W1–C2 44.08(61), C8–C6–W1–C2 –131.33(54), O6–C6–C8–C9 174.36(61), W1–C6–C8–C9 –9.41(91). D1: C8–C9–C10–C11–C12.

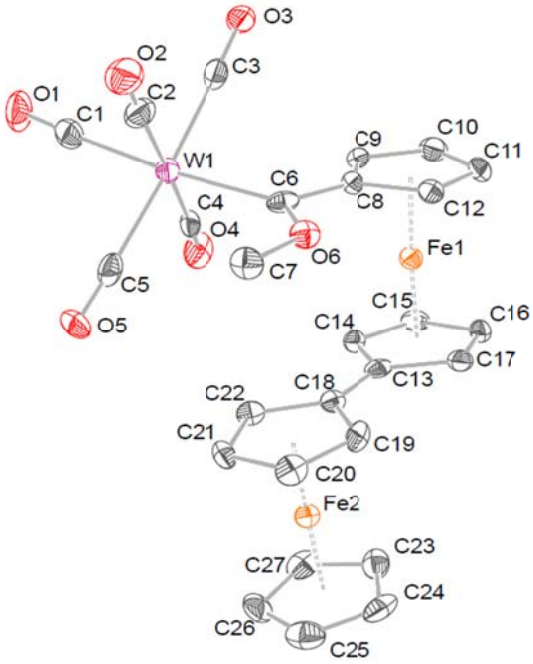

Figure 9. Single crystal X-ray structure analysis of **3** with the atom numbering scheme. Ellipsoids represent 50 % probability levels. Hydrogen atoms are omitted for clarity. Selected bond lengths (Å), angles (°), and torsion angles (°): W1–C1 2.034(56), W1-C6 2.207(49), C6-O6 1.335(51), C6-C8 1.457(71), D1–Fe1 1.653(7), D2–Fe1 1.662(7), O6-C6-W1 129.14(37), C8-C6-W1 123.69(31), O6-C6-C8 106.83(41), D1–Fe1–D2 176.25(5), C8–D1–D2–C13 –21.58(31), C18–D3–D4–C23 –0.27(33), D3–Fe2 1.6426(7), D4–Fe2 1.695(7), D3–Fe2–D4 166.47(5), W1–C6–O6–C7 6.92(58), C8–C6–O6–C7 –179.65(37), O6–C6–W1–C2 47.81(40), C8–C6–W1–C2 –124.63(38), O6–C6–C8–C9 172.42(41), W1–C6–C8–C9 –13.70(65), D1: C8–C9–C10–C11–C12, D2: C13–C14–C15–C16–C17, D3: C18–C19–C20–C21–C22, D4: C23–C24–C25–C26–C27.

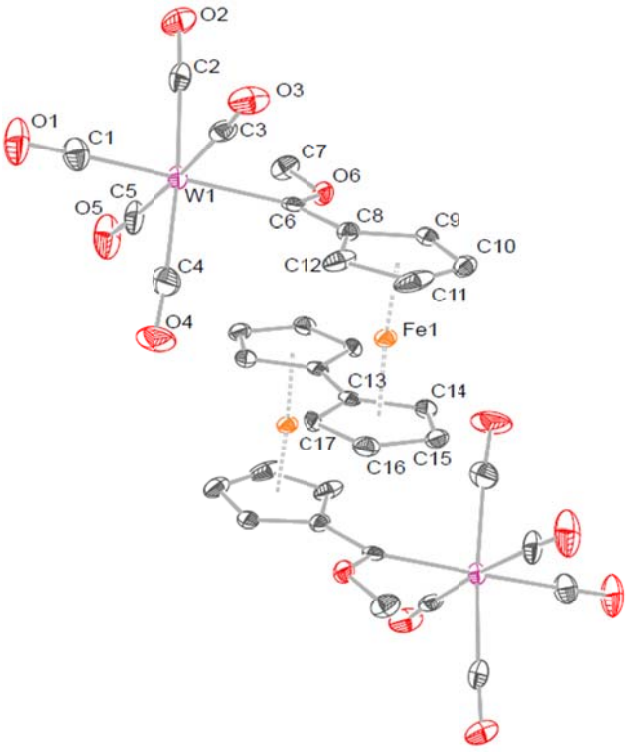

Figure 10. Single crystal X-ray structure analysis of **4** with the atom numbering scheme. Equivalent atoms are generated by the following symmetry operation: –x+2, –y, –z. Ellipsoids represent 50 % probability levels. Hydrogen atoms are omitted for clarity. Selected bond lengths (Å), angles (°), and torsion angles (°): W1–C1 2.022(37), W1-C6 2.217(31), C6-O6 1.317(38), C6-C8 1.456(44), D1–Fe1 1.649(5), D2–Fe1 1.658(5), O6-C6-W1 128.60(22), C8-C6-W1 123.87(23), O6-C6-C8 107.22(27), D1–Fe1–D2 175.72(4), C8–D1–D2–C13 22.60(22), W1–C6–O6–C7 –5.69(40), C8–C6–O6–C7 –179.39(26), O6–C6–W1–C2 –44.36(28), C8–C6–W1–C2 128.38(25), O6–C6–C8–C9 6.14(41), W1–C6–C8–C9 –167.93(23), D1: C8–C9–C10–C11–C12, D2: C13–C14–C15–C16–C17.

Suitable single crystals of **1** - **4** were obtained by slow evaporation of a saturated dichloromethane solution of the respective complex layered with *n*-hexane at –5 °C. The *ORTEP* diagrams with selected bond lengths (Å), bond angles (°), and torsion angles (°) are shown in Figures 7 – 10. The appropriate complexes crystallize in the orthorhombic space groups $Pca2_1$ (**1**) and *Pbcn* (**2**), the triclinic space group *P*–1 (**3**) and the monoclinic space group $P2_1/n$ (**4**) with one (**1**), a half (**2**,**4**) and four (**3**) molecules in the asymmetric unit.

Amongst the numerous solid state structures of Fischer carbene complexes, only six group VI alkoxyferrocenyl-substituted derivatives have been reported so far, whereby just one contains tungsten.[12c, 13b, 32]

In a comparison of the angles and bond distances (Figures 7 - 10) at the trigonal-planar carbene carbon, no further differences, not for the ferrocenyl unit nor for the biferrocenyls can be identified. W1–C1 distances are equal for all four complexes and coincide with the corresponding ethoxy-substituted derivative of **1**.[32] The free electron pairs at O6 are always directed towards the ferrocenyl moiety of the molecules, due to the electronic interaction with the carbonyl groups.[33] Thus, to avoid electronic interactions, the bonded methyl group C6 shields the oxygen atom O6. The carbene carbon and the C_5H_4 plane of the ferrocenyl moieties extend their π-system by arranging almost coplanar to each other. The highest deviations of the corresponding O6–C6–C8–C9 torsion angles can be found for one molecule in the asymmetric unit of **3** (10.99(39) °). Additionally, this plane shows a staggered orientation related to the carbonyl groups. The highest deviations from an ideally assumed angle (45 °) can be found in carbene **3**, which shows differences of 5.43(40) ° and 10.37(38) ° for the representing torsion angle O6–C6–W1–C2.

For the biferrocenyl complexes **3** and **4**, both ferrocenyl units are oriented in an antiparallel fashion with nearly or exactly coplanar C_5H_4 rings (highest deviation: 17.73(25) ° for **3** and 0.00(24) ° for **4**, respectively). Interestingly, carbene fragments are disposed synclinal and synperiplanar to the ferrocenyl substituent. This conformation strongly depends on the rotation of the cyclopentadienyl rings. Fischer carbenes **1** and **4** exhibit rather eclipsed than staggered torsion angles (–13.31(101) ° for **1** and 22.60(22) ° for **4**). In contrast, complex **2** with two tungsten carbene building blocks nearly shows an eclipsed conformation (3.69(63) °) for both C_5H_4 rings, whereby both fragments show synclinal orientation. The same conformation can also be found for the corresponding chromium complex with "propoxy substituents.[12] Torsion angles of both entities in the biferrocenyl unit of complex **3** are summarized in Table 5 showing great differences between the molecules (Table 5, A - D) of the asymmetric unit for the 1,1'-disubstituted moiety. Molecules B and C exhibit a nearly synclinal orientation, whereas A and D rather are arranged synperiplanar. However, all monosubsituted ferrocenyl fragments are synperiplanar oriented with small deviations for molecule B and D (Table 5).

Table 5. Torsion angles (°) for **3**.

Molecule	**C8–CT1–CT2–C13**	**C18–CT3–CT4–C23**
A	–21.61(29)	–0.70(31)
B	62.44(34)	–14.08(42)
C	–61.49(32)	–4.27(39)
D	15.65(29)	–16.22(29)

CONCLUSION

Within this study, a series of ferrocenyl (Fc = ferrocenyl; fc = ferrocen-1,1'-diyl) and biferrocenyl (Bfc = 1',1"-biferrocenyl; bfc = 1',1"-biferrocen-1,1'"diyl) tungsten Fischer carbene complexes, of type $[(CO)_5W{=}C(OMe)R]$ (**1**, R = Fc; **3**, R = Bfc) and $[(CO)_5W{=}C(OMe)\text{-}R'\text{-}(OMe)C{=}W(CO)_5]$ (**2**, R' = fc;

4, R' = bfc), is reported with the aim of investigating low energy charge transfer transitions between the transition metal carbonyl fragment and the (oxidized) carbene substituents. For this reason, ferrocenyl and biferrocenyl mono- and bismethox-bismethoxycarbene tungsten(0) complexes **1** – **4** were prepared and characterized spectroscopically in solution. Furthermore, the structural properties of **1** - **4** in the solid state were investigated by single-crystal X-ray diffraction studies whereby the biferrocenyl derivatives **3** and **4** exhibit a *syn*-conformation of ferrocenyl and carbene moiety. The results reveal no substituent effects in the bond-lengths and angles.

The electrochemical studies reveal reversible one electron redox events for the ferrocenyl/biferrocenyl moieties. Moreover, an electrochemical one electron transfer reaction could be found for the reduction of the Fischer carbene units. For the tungsten carbonyl moieties, irreversible oxidation processes could be detected. During the UV-Vis-NIR spectroelectrochemical investigations typical low energy absorptions for the mixed-valent biferrocenyl unit were found. A further observed high energy NIR absorption was attributed to a metal-metal charge transfer transition between the tungsten carbonyl increment and the ferrocenyl/biferrocenyl unit in the corresponding oxidized state and is reported herein for the first time. Finally, verification was made within infrared spectroelectrochemical studies by which the electronic interactions in the corresponding cationic species can be described as those of weakly coupled class II systems according to Robin and Day.

Experimental Section

General Information

All operations were carried out under an inert atmosphere of nitrogen or argon gas using standard Schlenk techniques. Solvents were dried by refluxing over sodium metal (*n*-hexane and tetrahydrofuran) or phosphorous pentoxide (dichloromethane) and were distilled under nitrogen prior to use. Chemicals were used without further purification unless stated elsewhere. Dibromobiferrocene was synthesized according to a literature procedure.[15] Tetra-*n*-butylammonium tetrakis(pentafluorophenyl)borate was prepared by metathesis of lithium tetrakis(pentafluorophenyl)borate etherate (Boulder Scientific) with tetra-*n*-butylammonium bromide according the a published procedure.[34] Purification with column chromatography was done using Silica gel 60 (0.0063 – 0.200mm) as stationary phase. A Bruker AVANCE 500 spectrometer was used for NMR recordings. ^{1}H NMR spectra were recorded at 500.30 MHz and $^{13}C\{^{1}H\}$ NMR spectra at 125.80 MHz. The signal of the solvent was used as reference: ^{1}H, $CDCl_3$ at 7.26 ppm and $^{13}C\{^{1}H\}$, $CDCl_3$ at 77.16 ppm. Infrared spectra were obtained with a Thermo Nicolet 200 FT-IR spectrometer using a NaCl cell and dichloromethane as solvent. Only the vibration bands in the carbonyl stretching region (1600 - 2200 cm^{-1}) were recorded. The melting points were determined using a Gallenkamp MFB 595 010 M melting point apparatus. Microanalyses were performed by using a Thermo FLASHEA 1112 Series instrument. High-resolution mass spectra were recorded with a Bruker micrOTOF QII with an Apollo II ESI source.

Synthesis of Fischer carbene complexes 1 – 4

$[(CO)_5W{=}C(OMe)Fc]$ (**1**)
Ferrocene (3.0 mmol, 0.56 g) was monolithiated according to a literature procedure in tetrahydrofuran (thf) with ^{t}BuLi (3.2 mmol).[14] The solution was cooled to -80 ^{o}C and $W(CO)_6$ (3.0 mmol, 1.06 g) was added in a single portion. The color of the solution turned deep red upon addition. The reaction mixture was stirred isotherm for 30 min and then allowed to reach room temperature within 1 h. The solvent was changed to dichloromethane (CH_2Cl_2), cooled to -50 ^{o}C and methyl trifluoromethanesulfonate (9.9 mmol, 1.09 mL) added. The reaction mixture was removed from the cold bath and stirred overnight at ambient temperature. Purification of the product was performed by using column chromatography and *n*-hexane as initial eluent. The polarity of the eluent was increased by adding small portions of CH_2Cl_2. Yield 1.44g (87%), dark red crystals. Anal. Calcd. for $C_{17}H_{12}FeO_6W$ (551.98): C, 36.99; H, 2.20; found C, 36.94; H, 2.12. Mp: 153°C. NMR ($CDCl_3$) ^{1}H: 4.99 (m, 2H, H_α), 4.84 (m, 2H, $H_ß$), 4.27 (s, 5H, Cp), 4.53 (s, 3H, CH_3). $^{13}C\{^{1}H\}$: 307.73($C_{carbene}$), 202.34(C_{trans}), 198.03(C_{cis}), 95.23(C_{ipso}), 75.06(C_α), 73.25($C_ß$), 70.80(Cp), 68.60(CH_3). IR ν(CO) (*n*-hexane): 2063 m (A_1''), 1974 w (B), 1946 s (A_1'), 1935 vs (E). FAB-MS [m/z]: 551.95 [M^+].

$[\{(CO)_5W{=}C(OMe)\}_2fc]$ (**2**)
Dilithiation of ferrocene (3.0 mmol, 0.56 g) was done according to methods previously reported with an 1:1 ^{n}BuLi/TMEDA solution in *n*-hexane (6.5 mmol) overnight at ambient temperature. Afterward, the solvent was removed by filtration via cannula and the remaining dilithioferrocene was redissolved in tetrahydrofuran. The resulting solution was cooled to -60 ^{o}C and $W(CO)_6$ (6.0 mmol, 2.11 g) was added in a single portion. After 1 h of isothermal stirring the solution was warmed up to room temperature within 60 min. All volatiles were removed, the residue was redissolved in CH_2Cl_2 and methyl trifluoromethanesulfonate (20.0 mmol, 2.41 mL) was added at -30 ^{o}C after which the reaction solution darkened. The resulting mixture was stirred overnight at ambient temperature. Purification of the crude product was performed by column chromatography using *n*-hexane as initial eluent. The polarity of the eluent was increased by adding small portions of dichloromethane. Yield 1.51g (85%), dark purple solid. Anal. Calcd. for $C_{24}H_{14}FeO_{12}W_2$ (917.91): C, 31.40; H, 1.54; found C, 30.92; H, 1.42. Mp: 195°C. NMR ($CDCl_3$) ^{1}H: 5.01 (m, 4H, H_α), 4.82 (m, 4H, $H_ß$), 4.54 (s, 6H, CH_3). $^{13}C\{^{1}H\}$: 310.72 ($C_{carbene}$), 202.07 (C_{trans}), 197.66 (C_{cis}), 96.07 (C_{ipso}), 76.58 (C_α), 74.93 ($C_ß$), 69.09 (CH_3). IR ν(CO) (*n*-hexane): 2063 m (A_1''), 1974 w (B), 1940 vs (A_1'overlap E). FAB-MS [m/z]: 917.89 [M^+].

$[(CO)_5W{=}C(OMe)Bfc]$ (**3**) and $[\{(CO)_5W{=}C(OMe)\}_2Bfc]$ (**4**)
Dibromobiferrocene[14,15] (3.0 mmol, 1.58 g) was dissolved in 50 mL of tetrahydrofuran and ^{n}BuLi (6.0 mmol) was added slowly at -40 ^{o}C. After 30 min of isothermal stirring, $W(CO)_6$ (6.0 mmol, 2.11 g) was added in a single portion. The solution was kept at -40 °C for an additional hour and then allowed to reach room temperature within 1 h. Afterward, the solvent was

changed to dichloromethane and methyl trifluoromethanesulfonate (20.0 mmol, 2.41 mL) was added at -30 °C. The reaction mixture was removed from the cold bath and stirred overnight at ambient temperature. Purification of the product was performed by column chromatography using *n*-hexane as initial eluent. The polarity of the eluent was increased by adding small portions of dichloromethane. Complexes **3** and **4** were purified and separated with column chromatography and gradient elution.

Compound **3**: Yield 0.96g (40%), red brown crystals. Anal. Calcd. for $C_{27}H_{20}Fe_2O_6W$ (736.01): C, 44.06; H, 2.74; found C, 43.95; H, 2.68. Mp: 166°C. NMR ($CDCl_3$) ^{1}H: 4.83 (m, 2H, $H_{ipso1\alpha}$), 4.64 (m, 2H, $H_{ipso1ß}$), 4.47 (m, 2H, $H_{ipso2\alpha}$), 4.32 (m, 2H, $H_{ipso2ß}$), 4.27 (m, 2H, $H_{ipso3\alpha}$), 4.26 (m, 2H, $H_{ipso3ß}$), 3.97 (s, 5H, Cp), 4.24 (s, 3H, CH_3). $^{13}C\{^1H\}$: 307.36($C_{carbene}$), 202.48(C_{trans}), 198.13(C_{cis}), 95.96(C_{ipso1}),88.24 (C_{ipso2}), 80.67 (C_{ipso3}), 75.06 ($C_{ipso1\alpha}$), 73.25($C_{ipso1ß}$), 70.17 ($C_{ipso2\alpha}$), 68.47($C_{ipso2ß}$), 68.12 ($C_{ipso3\alpha}$), 66.46($C_{ipso3ß}$), 69.43(Cp), 53.47(CH_3). IR ν(CO) (*n*-hexane): 2062 m (A_1''), 1972 w (B), 1943 s (A_1'), 1932 vs (E). FAB-MS [m/z]: 735.95 [M^+].

Compound **4**: Yield 0.99g (30%), dark brown crystals. Anal. Calcd. for $C_{36}H_{26}Fe_2O_{12}W_2$ (1101.94): C, 37.06; H, 2.02; found C, 37.08; H, 2.05. Mp: 232°C (decomp.). NMR ($CDCl_3$) ^{1}H: 4.83 (m, 4H, $H_{ipso1\alpha}$), 4.62 (m, 4H, $H_{ipso1ß}$), 4.44 (m, 4H, $H_{ipso2\alpha}$), 4.32 (m, 4H, $H_{ipso2ß}$), 4.30 (s, 6H, CH_3). $^{13}C\{^1H\}$: 308.72($C_{carbene}$), 202.29(C_{trans}), 198.03(C_{cis}), 96.05(C_{ipso1}),84.98 (C_{ipso2}), 75.98 ($C_{ipso1\alpha}$), 74.12($C_{ipso1ß}$), 70.70 ($C_{ipso2\alpha}$), 68.43($C_{ipso2ß}$), 67.97(CH_3). IR ν(CO) (*n*-hexane): 2062 m (A_1''), 1972 w (B), 1943 s (A_1'), 1932 vs (E). FAB-MS [m/z]: 1101.88 [M^+].

Electrochemistry. The electrochemical measurements were carried out under an argon atmosphere on 1.0 mmol·L^{-1} dichloromethane solutions containing 0.1 mol·L^{-1} of $[N^nBu_4][B(C_6F_5)_4]$ as supporting electrolyte utilizing a Voltalab 10 electrochemical laboratory from Radiometer analytical.[34] Furthermore, an OTTLE (= Optically Transparent Thin Layer Electrochemistry) cell placed in a Varian Cary 5000 UV-VIS/NIR absorption spectrometer or in a Thermo Nicolet 200 FT-IR spectrometer was used in spectroelectrochemical measurements.[18] For voltammetry, a three electrode cell with a platinum counter electrode, a glassy carbon working electrode and a Ag/Ag^+ reference electrode was used. The working electrode was prepared by polishing with a Buehler micro cloth using Buehler diamond pastes with decreasing sizes (1 to 0.25 μm). The Ag/Ag^+ reference electrode was constructed from a silver wire inserted into a luggin capillary with a vycor tip containing a solution of 0.01 mol·L^{-1} $AgNO_3$ as well as 0.1 mol·L^{-1} $[N^nBu_4][B(C_6F_5)_4]$ in acetonitrile. This luggin capillary was inserted into a second luggin capillary with vycor tip filled with a 0.1 mol·L^{-1} $[N^nBu_4][B(C_6F_5)_4]$ solution in dichloromethane. Successive experiments under the same experimental conditions showed that all formal reduction and oxidation potentials were reproducible within 5 mV. Experimentally potentials were referenced against a Ag/Ag^+ reference electrode but the results are presented referenced against the FcH/FcH^+ couple ($E_{1/2}$ = 0.0 V) as required by IUPAC.[35] When decamethylferrocene was used as an internal standard, the experimentally measured potential was converted in to *E vs* FcH/FcH^+ by addition of -0.61 V.[37] The cyclic voltammograms were taken after typical two scans and are considered to be steady state cyclic voltammograms, in which the signal pattern differs not from the initial sweep. Finally, the experimental data were processed on Microsoft Excel worksheets.

Computational Details. All quantum chemical calculations were performed with TURBOMOLE 6.3.1.[37] After the initial guess the Kohn-Sham equations were converged in the small def-SV(P)[38] basis set using a damping factor of 20 and Fermi smearing. After this step a geometry optimization was performed. Next the structures were optimized at the PB86/def2-TZVP[37,39] level of theory using the m5 grid. In all calculations density fitting was applied.[40] The final stationary points were characterized by analyzing the hessian matrix.[41] The final energy evaluations were performed with the B3LYP[38,42] hybrid functional in combination with the def2-TZVP basis set. To include the solvent effects the COSMO[43] solvation model with ε = ∞ was applied. The reported relative energies include the zero point energy correction from the gas phase at the BP86/def2-TZVP level of theory.

Single-Crystal X-ray Diffraction Analysis. Crystal data for **1** – **4** are summarized in Table SI-1 (Supporting Information). Data were collected with an Oxford Gemini S diffractometer at 100 K using Mo-Kα (λ = 0.71073 Å) radiation. The structures were solved by direct methods using SHELXS-97 and refined by full matrix least-square procedures on F2 using SHELXL-97.[44,45] All non-hydrogen atoms were refined anisotropically and a riding model was employed in the refinement of the hydrogen atom positions.

Crystallographic data (excluding structure factors) for the structures in this paper have been deposited with the Cambridge Crystallographic Data Centre, CCDC, 12 Union Road, Cambridge CB21EZ, UK. Copies of the data can be obtained free of charge on quoting the depository numbers CCDC-949877 (**1**), 949876 (**2**), 949878 (**3**) and 949875 (**4**) (Fax: +44-1223-336-033; E-Mail: deposit@ccdc.cam.ac.uk, http://www.ccdc.cam.ac.uk).

ASSOCIATED CONTENT

Supporting Information. UV-Vis/NIR spectra in dichloromethane and crystal structure details for **1** - **4** as well as calculated infrared spectra of **1** and $\mathbf{1}^+$ are given. This material is available free of charge via the Internet at http://pubs.acs.org.

AUTHOR INFORMATION

Corresponding Authors

Daniela I. Bezuidenhout: e-mail: daniela.bezuidenhout@up.ac.za; phone: +27-(0)12-420-2626; fax.: +27-(0)12-420-4687. Heinrich Lang: e-mail: heinrich.lang@chemie.tu-chemnitz.de; phone: +49 (0)371-531-21210; fax.: +49 (0)371-531-21219.

Author Contributions

The manuscript was written through contributions of all authors and all authors have given approval to the final version of the manuscript.

ACKNOWLEDGMENT

D.I.B. and B.v.d.W. acknowledge the National Research foundation, South Africa for financial support (Grant number 76226). We are grateful to the Fonds der Chemischen Industrie for financial support. J.M.S. and M.K. thank the FCI for Chemiefonds Fellowships.

REFERENCES

(1) (a) Fischer, E. O.; Maasböl, A. *Angew. Chem., Int. Ed. Engl.* **1964**, *3*, 580-581; (b) Bezuidenhout, D. I.; Lotz, S.; Liles, D. C.; van der Westhuizen, B.; *Coord. Chem. Rev.*, **2012**, *51*, 479-524; (c) Astruc, D. *Electron Transfer and Radical Processes in Transition Metal Chemistry*, VCH, New York, 1995; (d) Astruc, D. *Acc. Chem. Res.*, **1997**, *30*, 383-391; (e) Long, N. J. *Angew. Chem.,* **1995**, *34*, 21-38; (f) Behrens, U.; Brussaard, H.; Hagenau, U.; Heck, J.; Hendrickx, E.; Kornich, J.; van der Linden, J. G. M.; Persoons, A.; Spek, A. L.; Veldman, N.; Voss, B.; Wong, H. *Chem. Eur. J.* **1996**, *2*, 98-103.

(2) (a) Dötz, K. H. *Angew. Chem., Int. Ed. Engl.* **1975**, *14*, 644-645; (b) Aumann, R.; Heinen, H. *Chem. Ber.* **1987**, *120*, 537-540.

(3) Pike, A. R.; Ryder, L. C.; Horrocks, B. R.; Clegg, W.; Connolly, B. A.; Houlton, A. *Chem. Eur. J.*, **2004**, *11*, 344-353.

(4) Spanig, F.; Kolvacs, C.; Hauke, F.; Ohlubo, K.; Fukuzumi, F.; Guldi, D. M.; Hirsch, A. *J. Am. Chem. Soc.* **2009**, *131*, 8180-8195.

(5) (a) Shago, R. F.; Swarts, J. C.; Kreft, E.; Van Rensburg, C. E. J.; *Anticancer Res*. **2007**, *27*, 3431-3434; (b) Van Rensburg, C. E. J.; Kreft, E.; Swarts, J. C.; Dalrymple, S. R.; Macdonald, D. M.; Cooke, M. W.; Aquino, M. A. S. *Anticancer Res*. **2002**, *22*, 889-892; (c) Gross, A.; Hüsken, N.; Schur, J.; Raszeja, L.; Ott, I.; Metzler-Nolte, N. *Bioconjugate Chemistry*, **2012**, *23*, 1764-1774; (d) Swarts, J. C.; Vosloo, T. G.; Cronje, S. J.; Du Plessis, W. C.; Van Rensburg, C. E. J.; Kreft, E.; Van Lier, J. E. *Anticancer Res.* **2008**, *28*, 27812784; (e) Ott, I.; Kowalski, K.; Gust, R.; Maurer, J.; Mücke, P.; Winter, R. F. *Bioorg. Med. Chem. Lett.* **2010**, *20*, 866-869.

(6) See annual reviews by: Herndon, J. W. *Coord. Chem. Rev.,* 2002 – 2012.

(7) (a) Wulff, W. D. in *Advances in Metal-Organic Chemistry*; Liebeskind, L. S., Ed.; JAI Press Inc.: Greenwich, Conn, 1989; Vol. 1; b) Wulff, W. D., in "*Comprehensive Organic Synthesis*", Trost, B. M.; Fleming, I., Eds., Pergamon Press, 1990, Vol 5. c) Wulff, W. D. in *Comprehensive Organometallic Chemistry II*, Abel, E.W.; Stone, R.G.A.; Wilkinson, G., Eds.; Pergamon Press, 1995, *Vol. 12*, 469. d) Wulff, W. D., *Organometallics*, **1998**, *17*, 3116-3134.

(8) (a) Leroux, F.; Stumpt, R.; Fischer, H.; *Eur. J. Inorg. Chem.* **1998**, 1225-1234. (b) Licandro, E.; Maiorana, S.; Papagani, A.; Hellier, P.; Capella, L.; Persoons, A.; Houbrechts, S. *J. Organomet. Chem.* **1999**, *583*, 111-119. (c) Robin-Le Guen, F.; Le Poul, P.; Caro, B.; Pichon, R.; Kervarec, N.; *J. Organomet. Chem.* **2001**, *626*, 37-42. (d) Faux, N.; Caro, B.; Robin-Le Guen, F.; Le Poul, P.; Nakatani, K.; Ishow, E. *J. Organomet. Chem.* **2005**, *690*, 4982-4988. (e) Baldoli, C.; Cerea, P.; Falciola, L.; Giannini, C.; Licandro, F.; Maiorana, S.; Mussini, P.; Perdiccia, D.; *J. Organomet. Chem.* **2005**, *690*, 5777-5787.

(9) (a)Chandrasekhar, V.; Thirumoorthi, R. *Organometallics*, **2007**, *26*, 5415-5422; (b) Ogawa, S.; Muroaka, H.; Kikuta,K.; Saito, F.; Sato, R. *J. Organomet. Chem.*, **2007**, *692*, 60-69; (c) *Ferrocenes,* Stepnicka, P. Ed.; John Wiley & Sons, 2008; (d) Ludvik, J.; Stepnicka, P. *ECS Trans.,* **2007**, *2*, 17-25; (e) Hildebrandt, A.; Rüffer, T.; Erasmus, E.; Swarts, J. C.; Lang, H. *Organometallics*, **2010**, *29*, 4900-4905; (f) Speck, J. M.; Schaarschmidt, D.; Lang, H. *Organometallics* **2012**, *31*, 1975-1982.

(10) (a) Hildebrandt, A.; Lang, H. *Dalton Trans.* **2011**, *40*, 11831-11837; (b) Speck, J.M., Claus, R., Hildebrandt, A., Rüffer, T., Erasmus, E., van As, L., Swarts, J.C., Lang, H., *Organometallics*, **2012**, *31*, 6373-6380.

(11) (a) Connor, J. A.; Jones, E. M.; Lloyd, J. P. *J. Organomet. Chem.* **1970**, *24*, C20-C22; (b) Lloyd, M. K.; McCleverty, J. A.; Orchard, D. G.; Connor, J. A.; Hall, M. B.; Hillier, I. H.; Jones, E. M.; McEwen, G. K. *J. Chem. Soc., Dalton Trans.* **1973**, 1743-1747; (c) Casey, C. P.; Albin, L. D.; Saeman, M. C.; Evans, D. H. *J. Organomet. Chem.*, **1978**, *155*, C37-C40; (d) Limberg, A.; Lemos, M. A. N. D. A.; Pombeiro, A. J. L.; Maiorana, S.; Papagni, A.; Licandro, E.; *Port. Electrochim. Acta,* **1995**, *13*, 319-323; (e) Pombeiro, A. J. L. *New J. Chem.*, **1997**, *21*, 649-660; (f) Fernández, I.; Mancheño, M. J.; Gómez-Gallego, M.; Sierra, M. A.; *Org. Lett.*, **2003**, *5*, 1237-1240; (g) Martínez-Álvarez, R.; Gómez-Gallego, M.; Fernández, I.; Mancheño, M. J.; Sierra, M. A. *Organometallics*, **2004**, *23*, 4647-4654; (h) Wulff, W. D.; Korthals, K. A.; Martínez-Álvarez, R.; Gómez-Gallego, M.; Fernández, I.; Sierra, M. A. *J. Org. Chem.*, **2005**, *70*, 5269-5277; (i) López-Alberca, M. P.; Mancheño, M. J.; Fernández, I.; Gómez-Gallego, M.; Sierra, M. A.; Hemmert, C.; Gornitzka, K. H. *Eur. J. Inorg. Chem.*, **2011**, 842-849; (j) van der Westhuizen, B.; Swarts, P. J.; Strydom, I.; Liles, D. C.; Fernández, I.; Swarts, J. C.; Bezuidenhout, D. I. *Dalton Trans.* **2013**, 42, 5367-5378 (k) van der Westhuizen, B.; Swarts, P. J.; van Jaarsveld, L. M.; Liles, D. C.; Siegert, U.; Swarts, J. C.; Fernández, I.; Bezuidenhout, D. I. *Inorg. Chem.* **2013**, *52*, 6674-6684.

(12) (a) Bezuidenhout, D.I.; Lotz, S.; Landman, M.; Liles, D.C. *Inorg. Chem.* **2011**, *50*, 1521-1533; (b) Helten, H.; Beckman, M.; Schnakenburg, G.; Streubel, R. *Eur. J. Inorg. Chem.* **2010**, *16*, 2337-2341; (c) Bezuidenhout, D.I.; van der Watt, E.; Liles, D.C.; Landman, M.; Lotz, S. *Organometallics*, **2008**, *27*, 2447-2456; (d) Fischer, E.O.; Postnov, V.N.; Kreissl, F.R. *J. Organomet. Chem.*, **1982**, *23,* C73-C77.

(13) (a) Meca, L.; Dvorak, D.; Ludvik, J.; Cisarova, I.; Stepnicka, P. *Organometallics* **2004**, *23*, 2541-2551; (b) Butler, I.R.; Cullen, W.R.; Einstein, F.W.B.; Willis, A.C. *Organometallics*, **1985**, *4*, 603-604; (c) Fischer, E.O.; Gammel, F.J.; Besenhard, J.O.; Frank, A.; Neugebauer, D. *J. Organomet. Chem.,* **1980**, *191,* 261-282.

(14) R. Schobert, R. Kempe, T. Schmalz, A. Gmeiner, *J. Organomet. Chem*., **2006**, *691*, 859-868.

(15) Sünkel, K.; Bernhartzeder, S. *J. Organomet. Chem.* **2011**, *696*, 1536-1540.

(16) Dong, T.Y.; Chang, C.K.; Lee, S.H.; Lai, L.L.; Chiang, M.Y.N.; Lin, K.L. *Organometallics,* **1997**, *16*, 5816-5825.

(17) *Spectral Database for Organic Compounds (SDBS)*; ^{1}H NMR spectrum (No. 6650HPM-00-130); SDBS No.: 6650; RN: 102-54-5; http://riodb01.ibase.aist.go.jp/sdbs/.

(18) Krejčik, M.; Daněk, M.; Hartl, F. *J. Electroanal. Chem.* **1991**, *317*, 179-187.

(19) Cardona, C. M.; Li, W.; Kaifer, A. E.; Stockdale, D.; Bazan, G. C. *Adv. Mater.* **2011**, *23*, 2367-2371.

(20) Baldoli, C.; Cerea, P.; Falciola, L.; Giannini, C.; Licandro, E.; Maiorana, S.; Mussini, P.; Perdicchia, D. *J. Organomet. Chem.* **2005**, *690*, 5777-5787.

(21) (a) Bott, A. W.; Heineman, W. R. *Curr. Sep.* **2004**, *20*, 121-126; (b) Anson, F. C.; Christie, J. H.; Osteryoung, R. A. *J. Electroanal. Chem.* **1967**, *13*, 343-353.

(22) Bezuidenhout, D. I.; Barnard, W.; Van der Westhuizen, B.; Van der Watt, E.; Liles, D. C. *Dalton Trans.* **2011**, *40*, 6711-6721.

(23) Camire, N.; Mueller-Westerhoff, U. T.; Geiger, W. E. *J. Organomet. Chem.* **2001**, *637*, 823-826.

(24) Robin, M. B.; Day, P. *Adv. Inorg. Chem. Radiochem.* **1968**, *10*, 247-422.

(25) (a) Connor, J. A.; Lloyd, J. P. *J. Chem. Soc., Dalton Trans.* **1972**, 1470-1476; (b) Rosenblum, M.; Santer, J. O.; Howells, W. G. *J. Am. Chem. Soc.* **1957**, *85*, 1450-1458; (c) Sohn, Y. S.; Hendrickson, D. N.; Gray, H. B. *J. Am. Chem. Soc.* **1971**, *93*, 3603-3612.

(26) Warratz, R.; Aboulfadl, H.; Bally, T.; Tuczek, F. *Chem. Eur. J.* **2009**, *15*, 1604-1617.

(27) (a) Atwood, C. G.; Geiger, W. E. *J. Am. Chem. Soc.* **1994**, *116*, 10849-10850; (b) Lohan, M.; Ecorchard, P.; Rüffer, T.; Justaud, F.; Lapinte, C.; Lang, H. *Organometallics* **2009**, *28*, 1878-1890; (c) Paul, F.; Toupet, L.; Thépot, J.-Y.; Costuas, K.; Halet, J.-F.; Lapinte, C. *Organometallics* **2005**, *24*, 5464-5478.

(28) (a) D'Alessandro, D. M.; Keene, F. R. *Chem. Soc. Rev.* **2006**, *35*, 424-440; (b) Brunschwig, B. S.; Creutz, C.; Sutin, N. *Chem. Soc. Rev.* **2002**, *31*, 168-184.
(29) Warratz, R.; Tuczek, F. *Inorg. Chem.* **2009**, *48*, 3591-3607.
(30) (a) Siebler, D.; Förster, C.; Gasi, T.; Heinze, K. *Organometallics* **2011**, *30*, 313-327; (b) Lohan, M.; Justaud, F.; Roisnel, T.; Ecorchard, P.; Lang, H.; Lapinte, C. *Organometallics* **2010**, *29*, 4804-4817.
(31) Dong, T.-Y.; Lee, T.-Y.; Lee, S.-H.; Lee, G.-H.; Peng, S.-M. *Organometallics* **1994**, *13*, 2337-2348.
(32) López-Cortés, J. G.; Contreras de la Cruz, L. F.; Ortega-Alfaro, M. C.; Toscano, R. A.; Alvarez-Toledano, C.; Rudler, H. *J. Organomet. Chem.* **2005**, *690*, 2229-2237.
(33) Fernández, I.; Cossío, F. P.; Arrieta, A.; Lecea, B.; Mancheño, M. J.; Sierra, M. A. *Organometallics* **2004**, *23*, 1065-1071.
(34) (a) LeSuer, R. J.; Buttolph, C.; Geiger, W. E. *Anal. Chem.* **2004**, *76*, 6395-6401; (b) Barrière, F.; Camire, N.; Geiger, W. E.; Mueller-Westerhoff, U. T.; Sanders, R. *J. Am. Chem. Soc.* **2002**, *124*, 7262-7263; (c) Barrière, F.; Geiger, W. E. *J. Am. Chem. Soc.* **2006**, *128*, 3980-3989.
(35) Gritzner, G.; Kuta, J. *Pure Appl. Chem.* **1984**, *56*, 461-466.
(36) Nafady, A.; Geiger, W. E. *Organometallics* **2008**, *27*, 5624-5631.
(37) (a) TURBOMOLE V6.3 2011, a development of University of Karlsruhe and Forschungszentrum Karlsruhe GmbH, since 2007; available from http://www.turbomole.com., 1989-2007; (b) Haser, M.; Ahlrichs, R. *J. Comput. Chem.* **1989**, *10*, 104-111; (c) Deglmann, P.; Furche, F.; Ahlrichs, R. *Chem. Phys. Lett.* **2002**, *362*, 511-518; (d) van Wüllen, C. *J. Comp. Chem.* **2002**, *32*, 1195-1201.
(38) (a) Weigend, F.; Ahlrichs, R. *Phys. Chem. Chem. Phys.* **2005** , *7*, 3297-3305; (b) Weigend, F.; Häser, M.; Patzelt, H.; Ahlrichs, R. *Chem. Phys. Lett.* **1998**, *294*, 143-152; (c) Schäfer, A.; Horn, H.; Ahlrichs, R. *J. Chem. Phys.* **1992** , *97*, 2571-2522.
(39) (a) Becke, A. D. *Phys. Rev. A* **1988**, *38*, 3098-3100; (b) Perdew, J.P. *Phys. Rev. B* **1986**, *33*, 8822-8824.
(40) (a) Weigend, F. *Phys. Chem. Chem. Phys.* **2006**, *8*, 1057-1065; (b) Eichkorn, K.; Treutler, O.; Oehm, H.; Häser, M.; Ahlrichs, R. *Chem. Phys. Lett.* **1995**, *242*, 652-660; (c) Eichkorn, K.; Weigand, F.; Treutler, O.; Ahlrichs, R. *Theo. Chem. Acc.* **1997**, *97*, 119-124.
(41) (a) Treutler, O.; Ahlrichs, R. *J. Chem. Phys.* **1995**, *102*, 346-354; (b) v. Arnim, M.; Ahlrichs, R. *J. Chem. Phys.* **1999**, *111*, 9183-9190.
(42) (a) Lee, C.; Yang, W.; Parr, R. G. *Phys. Rev. B* **1988**, *37*, 785-789; (b) Becke, A. D. *J. Chem. Phys.* **1993**, *98*, 5648-5652.
(43) Klamt, A.; Schüürmann, G. *J. Chem. Soc., Perkin Trans.* **1993**, *2*, 799-805.
(44) Sheldrick, G. M. *Acta Crystallogr., Sect. A* **1990**, *46*, 467.
(45) Sheldrick, G. M. SHELXL-97, Program for Crystal Structure Refinement; Universität Göttingen, Göttingen, Germany, 1997.

SUPPORTING INFORMATION

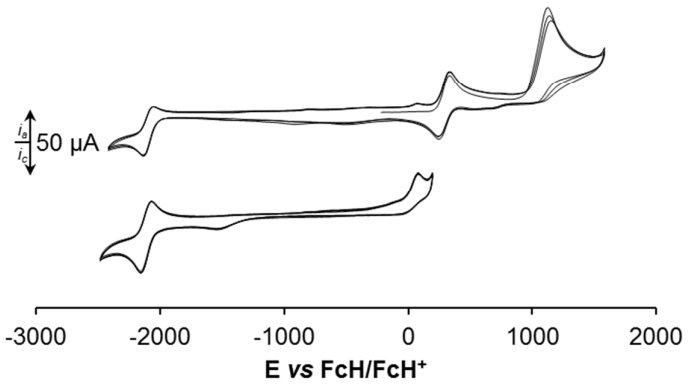

Figure SI-1. Cyclic voltammograms (multi scan) of **1.** Scan rates: 100 mVs^{-1} (top) and 500 mV^{-1} (bottom) in dichloromethane solutions (1.0 mmol.L-1) at 25 °C, supporting electrolyte $[N^nBu_4][B(C_6F_5)_4]$ (0.1 M).

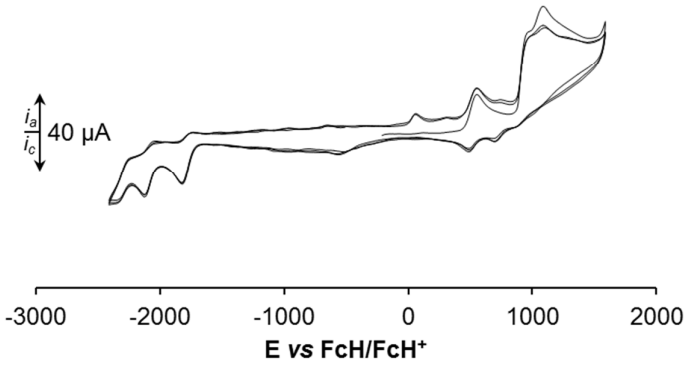

Figure SI-2. Cyclic voltammogram (multi scan) of **2.** Scan rate: 100 mVs^{-1} in dichloromethane solutions (1.0 mmol.L-1) at 25 °C, supporting electrolyte $[N^nBu_4][B(C_6F_5)_4]$ (0.1 M).

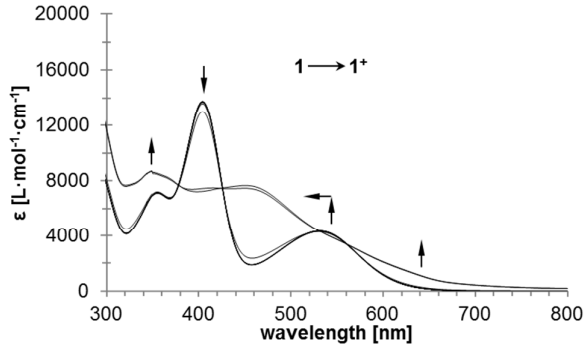

Figure SI-3. UV-Vis spectra of **1** at rising potentials (0 to 700 mV). All potentials *vs* Ag/AgCl at 25 °C in dichloromethane, supporting electrolyte $[N^nBu_4][B(C_6F_5)_4]$ (0.1 M). Arrows indicate increasing or decreasing as well as shifting absorptions.

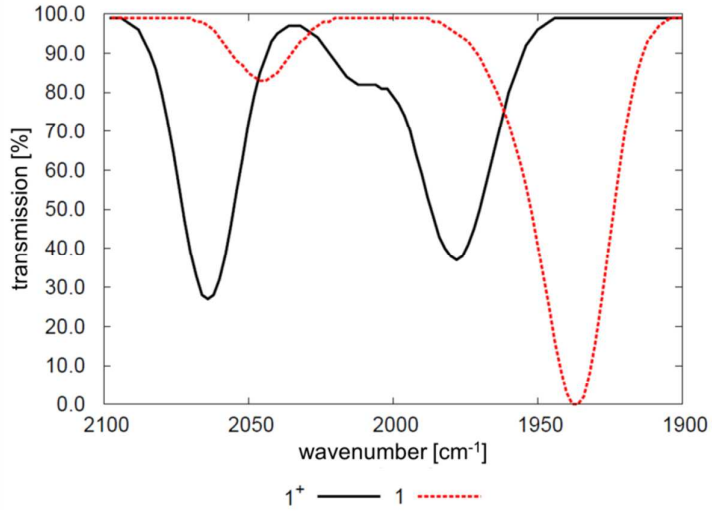

Figure SI-4. Calculated ν(CO) stretching frequencies of **1** and **1**$^+$. Computational details are given in the Experimental Section.

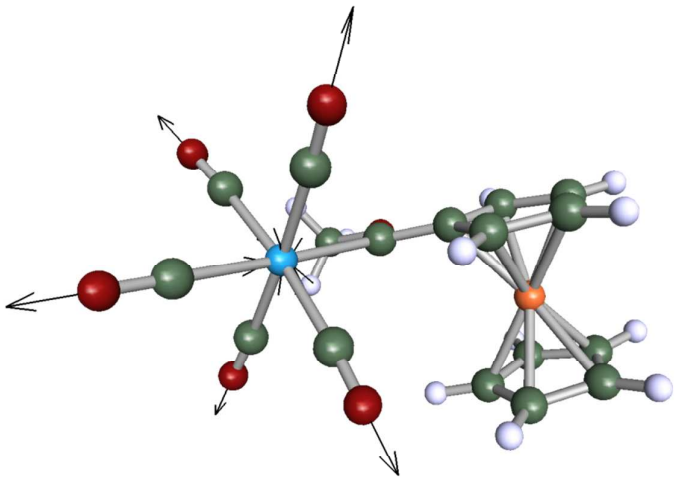

Figure SI-5. Visualization of calculated ν(CO) vibration mode for **1** at 2045 cm^{-1} (A_1", Figure SI-2).

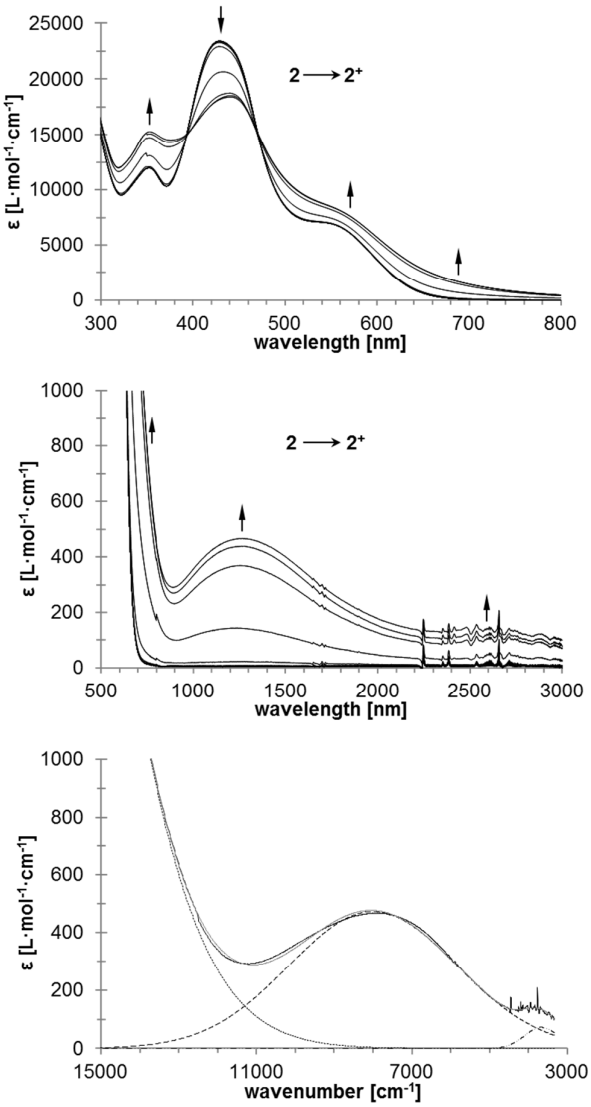

Figure SI-6. UV-Vis/NIR spectra of **2** at rising potentials (-100 to 1000 mV). Top: 300 – 800 nm. Middle: 500 – 3000 nm. Bottom: deconvolution of NIR absorptions at 1000 mV, using three distinct overlapping transitions with Gaussian shapes (dashed line indicates MMCT absorptions, dotted line corresponds to absorptions caused by interactions between ligand and metal, dotted dashed line represents ligand field transitions). All potentials *vs* Ag/AgCl at 25 °C in dichloromethane, supporting electrolyte $[N^{n}Bu_4][B(C_6F_5)_4]$ (0.1 M). Arrows indicate increasing or decreasing as well as shifting absorptions.

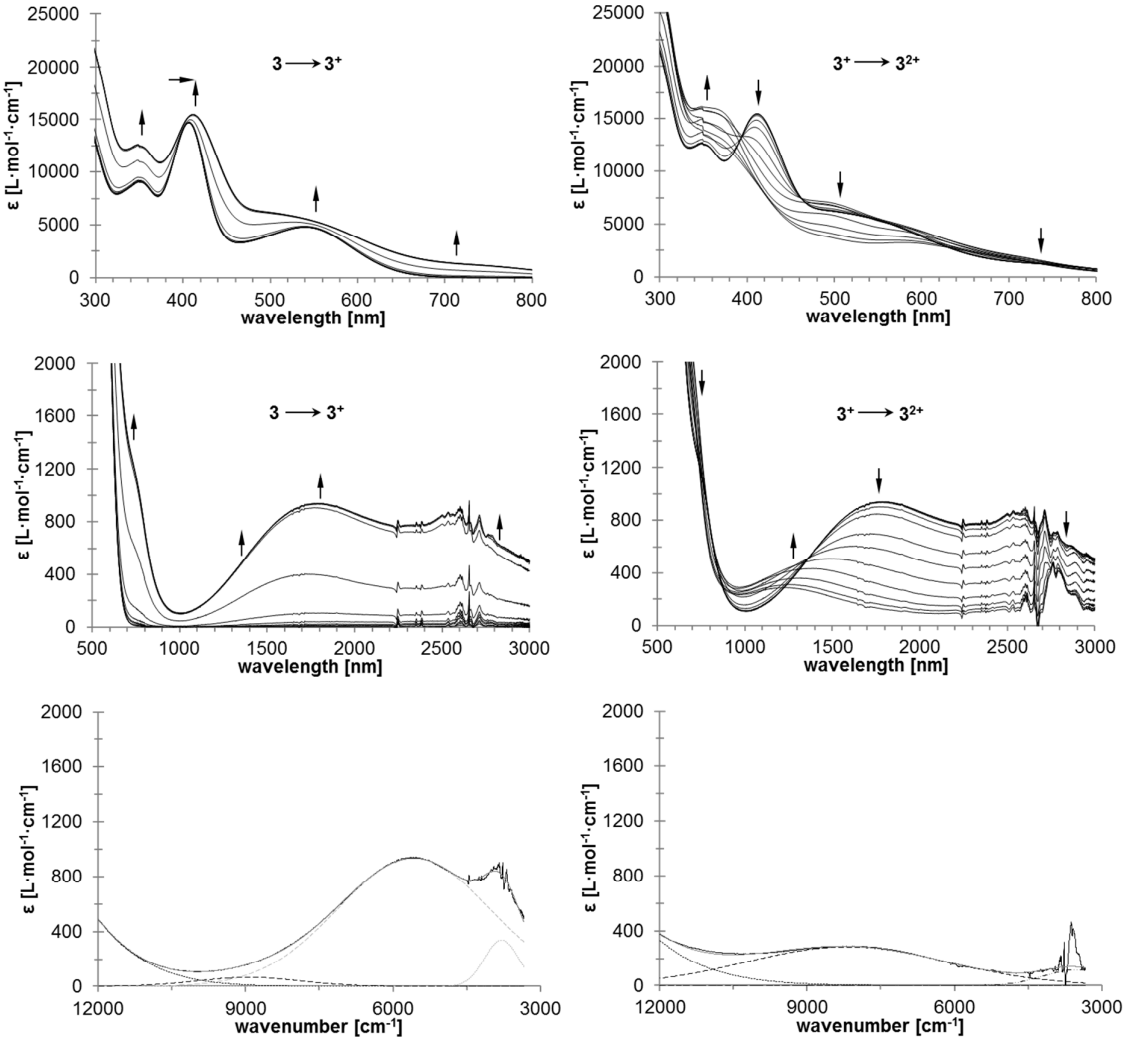

Figure SI-7. UV-Vis/NIR spectra of **3** at rising potentials (left: -100 to 400 mV; right: 400 to 1000 mV). Top: 300 – 800 nm. Middle: 500 – 3000 nm. Bottom (left): deconvolution of NIR absorptions at 400 mV, using three distinct overlapping transitions with Gaussian shapes. Bottom (right): deconvolution of NIR absorptions at 1000 mV, using three distinct overlapping transitions with Gaussian shapes (dashed line indicates IVCT (grey) or MMCT (black) absorptions, dotted line corresponds to absorptions caused by interactions between ligand and metal (black) as well as intrabiferrocenyl transitions (IBT, grey), dotted-dashed line represents ligand field transitions). All potentials *vs* Ag/AgCl at 25 °C in dichloromethane, supporting electrolyte $[N^{n}Bu_4][B(C_6F_5)_4]$ (0.1 M). Arrows indicate increasing or decreasing as well as shifting absorptions.

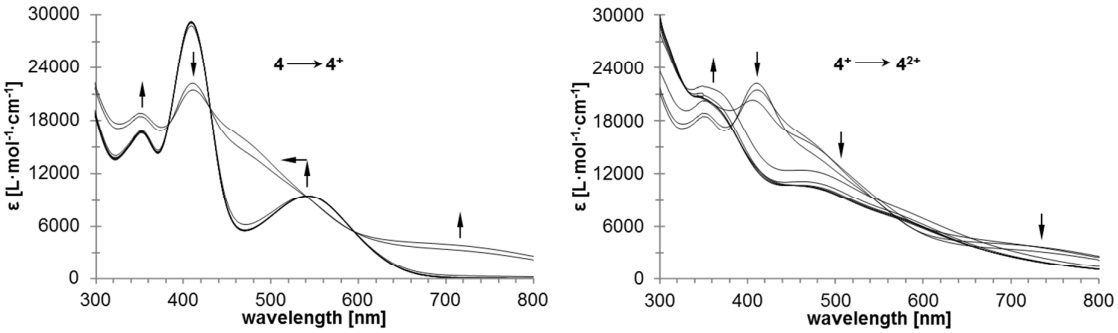

Figure SI-8. UV-Vis spectra of **4** at rising potentials (left: -100 to 600 mV; right: 600 to 1050 mV). All potentials *vs* Ag/AgCl at 25 °C in dichloromethane, supporting electrolyte $[N^{n}Bu_4][B(C_6F_5)_4]$ (0.1 M). Arrows indicate increasing or decreasing as well as shifting absorptions.

Table SI-1. Data Collection and Crystal Structure Details for **1** – **4.**

	1	**2**	**3**	**4**
Chemical formula	$C_{17}H_{12}FeO_6W$	$C_{24}H_{14}FeO_{12}W_2$	$C_{27}H_{20}Fe_2O_6W$	$C_{34}H_{22}Fe_2O_{12}W_2$
Formula weight	551.97	917.90	735.98	1101.92
Crystal system, space group	orthorhombic, $Pca2_1$	orthorhombic, *Pbcn*	triclinic, *P–1*	monoclinic, $P2_1/n$
a [Å]	20.2216(14)	13.5817(8)	7.2565(3)	10.4968(3)
b [Å]	6.9527(5)	14.2798(8)	22.2626(7)	13.1509(3)
c [Å]	11.7231(9)	13.2044(6)	31.8703(10)	11.9019(3)
α, β, γ [°]			105.358(3), 95.673(3), 98.626(3)	97.546(2)
V [Å^3]	1648.2(2)	2560.9(2)	4856.5(3)	1628.74(7)
$\rho_{calc.}$ [g cm^{-3}]	2.224	2.381	2.013	2.247
F(000)	1048	1712	2848	0.71073 A
Crystal dimensions [mm]	0.4 x 0.2 x 0.05	0.4 x 0.4 x 0.01	0.40 x 0.28 x 0.02	0.40 x 0.40 x 0.40
Z	4	4	8	2
Max., min. transmission	1.000, 0.592	1.000, 0.386	0.890, 0.200	0.1426, 0.1426
μ [mm^{-1}]	7.884	9.585	5.946	7.979
θ [°]	3.10–25.25	3.09–25.23	2.90–25.25	3.10–25.24
Index ranges	$-24 \le h \le 20$	$-10 \le h \le 16$	$-8 \le h \le 8$	$-12 \le h \le 12$
	$-5 \le k \le 8$	$-17 \le k \le 17$	$-26 \le k \le 26$	$-15 \le k \le 15$
	$-13 \le l \le 14$	$-15 \le l \le 15$	$-38 \le l \le 38$	$-11 \le l \le 14$
Total/unique reflections	6596/2749	8750/2302	45035/17555	11708/2938
Completeness to F^2	98.5 %	99.2 %	99.7 %	99.2 %
Data/restraints/parameters	2749/371/227	2302/308/182	17555/466/1297	2938/121/226
R_{int}	0.0510	0.0726	0.0405	0.0332
R_1, wR_2, $[I \ge 2\sigma(I)]$	0.0519, 0.1287	0.0564, 0.1372	0.0356, 0.0760	0.0184, 0.0414
R_1, wR_2 (all data)	0.0581, 0.1337	0.0673, 0.1457	0.0463, 0.0802	0.0204, 0.0422
Goodness-of-fit (S) on F^2	1.061	1.049	1.033	1.075
Largest diff. peak and hole [e Å^{-3}]	4.828, –1.400	2.760, –1.980	2.662, –1.273	0.562, –0.487

Absolute structure parameter[1]: 0.30(2) for **1.**

References

(1) Flack, H. D. *Acta Cryst., Sect. A*, **1983**, *39*, 876.

For Table of Contents only

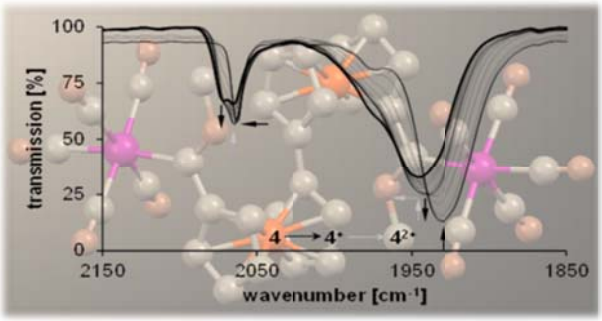

The syntheses, structures and UV-Vis-NIR spectroelectrochemical analyses of novel mono- and biscarbene tungsten complexes of ferrocene and biferrocene are presented. The order of the different oxidation processes could be established, while the NIR spectra recorded provided evidence for the first time, for charge transfer metal-metal interaction between the mixed-valent tungsten(0) pentacarbonyl moieties and the ferrocenyl/biferrocenyl carbene substituents. This was confirmed with the spectroelectrochemical investigation and by use of DFT calculations.